Journal of Sedimentary Research

Journal of Sedimentary Research, 2015, v. 85, 459–488
Research Article
DOI: http://dx.doi.org/10.2110/jsr.2015.26

TECTONICALLY CONTROLLED NEARSHORE DEPOSITION: COZZETTE SANDSTONE, BOOK CLIFFS, COLORADO, U.S.A.

ANDREW S. MADOF,[1] NICHOLAS CHRISTIE-BLICK,[2] AND MARK H. ANDERS[2]
[1]*Chevron Energy Technology Company, Houston, Texas 77002-7308, U.S.A.*
[2]*Department of Earth and Environmental Sciences and Lamont-Doherty Earth Observatory of Columbia University, Palisades, New York 10964-8000, U.S.A.*
e-mail: andrew.madof@chevron.com

ABSTRACT: **The Book Cliffs of eastern Utah and western Colorado have been pivotal in the development of outcrop-based sequence stratigraphic concepts for nonmarine to shallow marine siliciclastic depositional settings. Prior studies in this area, and more generally in the Cretaceous western interior foreland basin of North America, have concluded that nearshore accumulation is controlled for the most part by the interaction between oscillatory eustatic change and longer-term regional patterns of flexural subsidence. New outcrop and subsurface evidence reported here from the eastern Book Cliffs suggests that three-dimensional tectonic tilting at length scales of up to ~ 50 km (31 mi) and timescales of less than ~ 200 kyr also strongly influenced sedimentation. Continental ice sheets are thought to have been small at the time. Documented patterns of accumulation are inconsistent with those expected from interactions of eustasy and regional flexure alone.**

The upper Campanian Cozzette Sandstone Member of the Mount Garfield Formation consists of twelve lithofacies arranged into six lithofacies assemblages, inferred to have been deposited in shallow marine, marginal marine, and nonmarine depositional environments. Shallow marine facies are organized into six wedge-shaped units < 40 m thick, bounded by flooding surfaces, and separated into three larger-scale cycles, which display along-strike and time-equivalent aggradational and progradational stacking. These successions are interpreted as shoreface–foreshore–swamp parasequences, and are erosionally overlain by fluvial and estuarine deposits. Both fluvial and estuarine accumulations are underlain by composite erosional surfaces, belonging either to two distinct incised-valley fills or to one composite fill. The proposed interpretation is based on high-resolution correlations made from digital video and continuous photographs acquired during a helicopter survey of the member. This interpretation differs significantly from published cross sections of the Cozzette, in which the sandstone is inferred to consist of at least two sheet-like shallow marine parasequences, truncated by sequence boundaries.

Facies variations, stratigraphic thickness trends, and geometrical relationships reveal that three basinward–landward cycles of syndepositional to postdepositional tectonic tilting in the southern Piceance basin controlled accumulation in the Cozzette Sandstone. Differential subsidence to the southeast led to the development of a northeast-trending clinoform rollover. Subsequent tilting to the north resulted in renewed accommodation creation, and reorientation of the rollover to an eastward trend. Following deposition of six shallow marine parasequences, tilting towards the northeast resulted in bypass and the development of a sequence boundary. The main conclusion of our study, that nearshore sedimentation was modulated by local tectonism at timescales of less than hundreds of thousands of years, casts doubt on the generally accepted eustatic paradigm at a location that was among the most important in the development of sequence stratigraphic concepts.

INTRODUCTION

Nearshore accommodation has long been assumed to be controlled by a combination of eustatic oscillation and regional subsidence at generally longer timescales (Mitchum et al. 1977; Vail et al. 1977; Van Wagoner 1985, 1995; Haq et al. 1987, 1988; Vail 1987; Posamentier et al. 1988; Posamentier and Vail 1988; Van Wagoner et al. 1990; Mitchum and Van Wagoner 1991; Posamentier et al. 1992; Posamentier and Allen 1993; Catuneanu et al. 2000). According to this view, systems tracts containing nonmarine to shallow marine facies, as well as their bounding surfaces, are related conceptually to specific portions and points on a relative-sea-level curve. Tectonically simple settings such as passive continental margins and tectonically active basins (e.g., retroarc foreland basins) are both assumed to subside differentially and in comparable ways (Posamentier and Allen 1993; Martinson et al. 1998; Willis 2000; Varban and Plint 2008), though with foreland subsidence depending primarily on proximity to the thrust load rather than on crustal thinning. As a result, it has been argued that the rate of subsidence in foreland basins exceeds the rate of eustatic falls consistently in areas proximal to the orogenic belt, but only episodically in regions distal to the thrust load (Posamentier and Allen 1993; Willis 2000; Castle 2001; Hoy and Ridgway 2003; Escalona and Mann 2006; Bera et al. 2008).

Outcrop and well-log data collected from the synorogenic Cozzette Sandstone Member of the Mount Garfield Formation in the eastern Book Cliffs of western Colorado (Figs. 1, 2), southern Piceance basin, have been used to test the hypothesis that deposition in the Late Cretaceous western interior foreland basin was modulated by the interaction of eustatic change and regional patterns of flexural subsidence in the manner

Published Online: May 2015
 1527-1404/15/085-459/$03.00

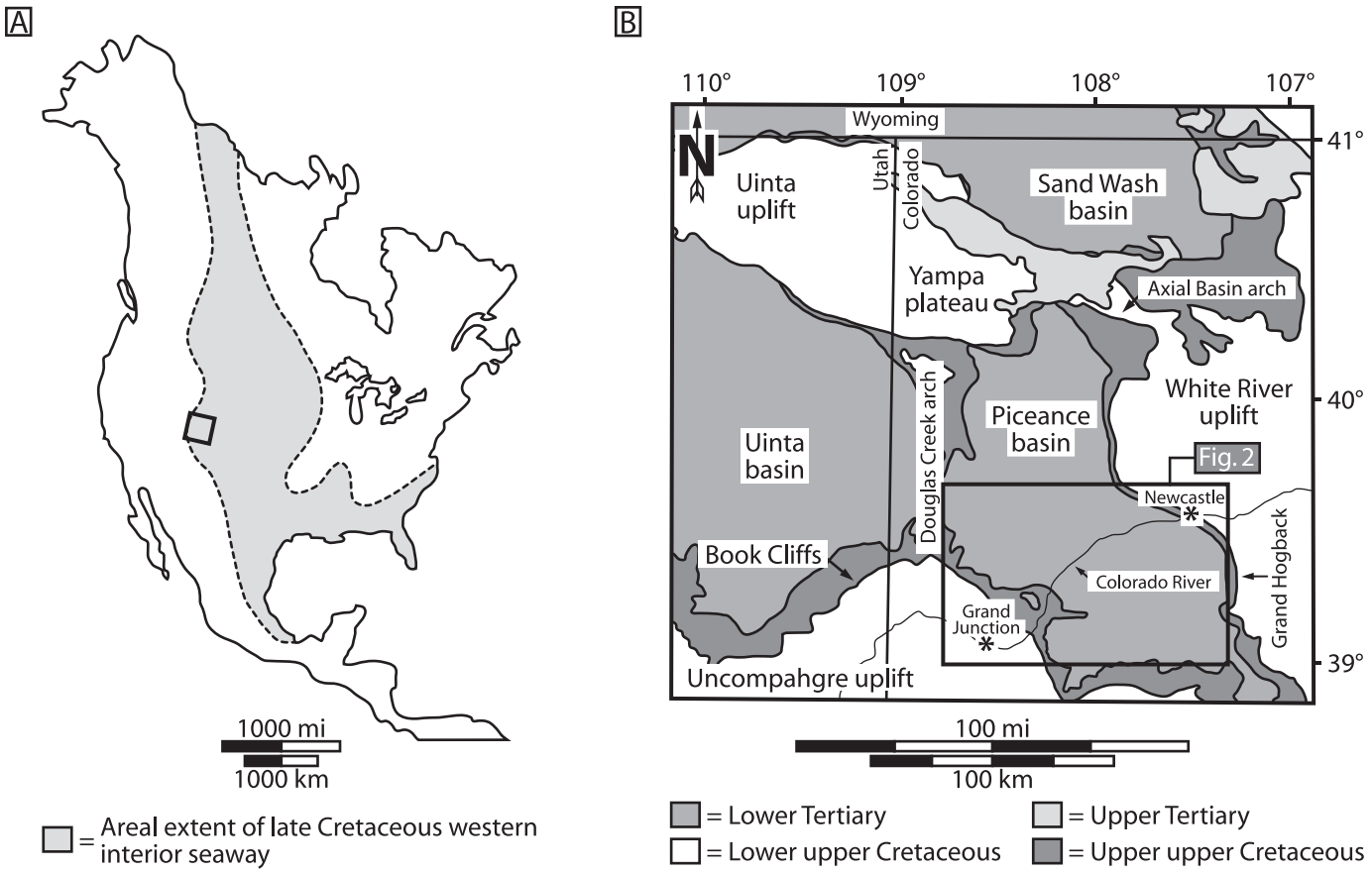

FIG. 1.—**A)** Paleogeographic map of North America showing areal extent of Late Cretaceous western interior seaway (modified from Van Wagoner 1995). Box on western margin is shown in detail in Part B. **B)** Geologic map showing major tectonic elements and ages of deposits in southern Wyoming, eastern Utah, and western Colorado (modified from Zapp and Cobban 1960). Box in southern Piceance basin delineates study area.

that is generally accepted. Available age control allows a comparison between late Campanian sea-level change (e.g., Miller et al. 2005a) and the timing of syndepositional thrusting (e.g., DeCelles et al. 1995; DeCelles and Coogan 2006). Stratal geometry, thickness trends, and patterns of facies variation in the Cozzette provide a basis for evaluating local controls on accumulation.

The Mount Garfield Formation, as well as other Cretaceous units in the Piceance basin, has received considerable attention for commercial coal (Erdmann 1934; Fisher 1936; Collins 1976; Van Wagoner 1991a) and natural-gas production (Warner 1964; Johnson 1989; Patterson et al. 2003; Cumella and Scheevel 2008; Hood and Yurewicz 2008; Yurewicz et al. 2008). The Cameo coal, no more than a few tens of meters above the top of the formation, was once the most economic coal zone in the basin (Young 1966; Johnson 1989). Rocks of the Mount Garfield Formation include low-permeability and low-porosity gas reservoirs sourced from interbedded coals and marine shales (Johnson 1989; Patterson et al. 2003). Existing estimates suggest that the Piceance basin contains approximately 112×10^9 kg (124 billion tons) of coal in beds over 1.2 m (4 ft) thick (Collins 1976), and from 2.8 to 7.1×10^9 m^3 (100 to 250 trillion cubic feet) of gas, principally in fluvial strata of the overlying Williams Fork Formation (Hood and Yurewicz 2008).

TECTONIC SETTING

The Cozzette Sandstone accumulated in a retroarc foreland basin setting east of the Sevier orogen and at the western margin of the Late Cretaceous western interior seaway (Fig. 1A; Van Wagoner 1995; Hettinger and Kirschbaum 2003; Kirschbaum and Hettinger 2004). The seaway, which extended more than 4,800 km (2,983 mi) from the Canadian Arctic to the Gulf of Mexico, and was as wide as 1,600 km (1,000 mi) between central Utah and Iowa (Jordan 1981; Robinson Roberts and Kirschbaum 1995), is thought to reflect subduction dynamics as well as crustal loading (Cross 1986; Burgess et al. 1997; Liu and Nummendal 2007). Subduction of a postulated aseismic ridge (Henderson et al. 1984) during late Campanian time is hypothesized to have reduced the dip of the Farallon plate (Dickinson and Snyder 1978), and to have resulted in sublithospheric loading and cooling and in rapid subsidence over an anomalously broad area (Cross 1986). At the same time, the transmission of tectonic stresses into the interior of the continent led to thick-skinned thrusting and to reorganization and segmentation of the foreland basin (the basement-involving Laramide phase of deformation; DeCelles 2004). Partitioning of the foreland into smaller basins, which include the Piceance of northwestern Colorado, persisted into Eocene time (Johnson 1989; Patterson et al. 2003).

The Piceance is an elongate structural basin (Collins 1976) with a map-view area of approximately 14,244 km^2 (5,500 mi^2; Fig. 1B; Hood and Yurewicz 2008) and a Cambrian through Eocene stratigraphic thickness of more than 8,250 m (27,000 ft; Yurewicz et al. 2008). The basin is bounded by the Axial Basin arch (north), the White River uplift and the Grand Hogback (east), the Uncompaghre uplift (southwest), the Douglas Creek arch (west), and the Uinta uplift (northwest; Collins 1976; Johnson 1989; Patterson et al. 2003). The Book Cliffs escarpment serves as the erosional southern limit to the Uinta and Piceance basins, which together mark the northern flank of the Colorado plateau (Young 1966). The

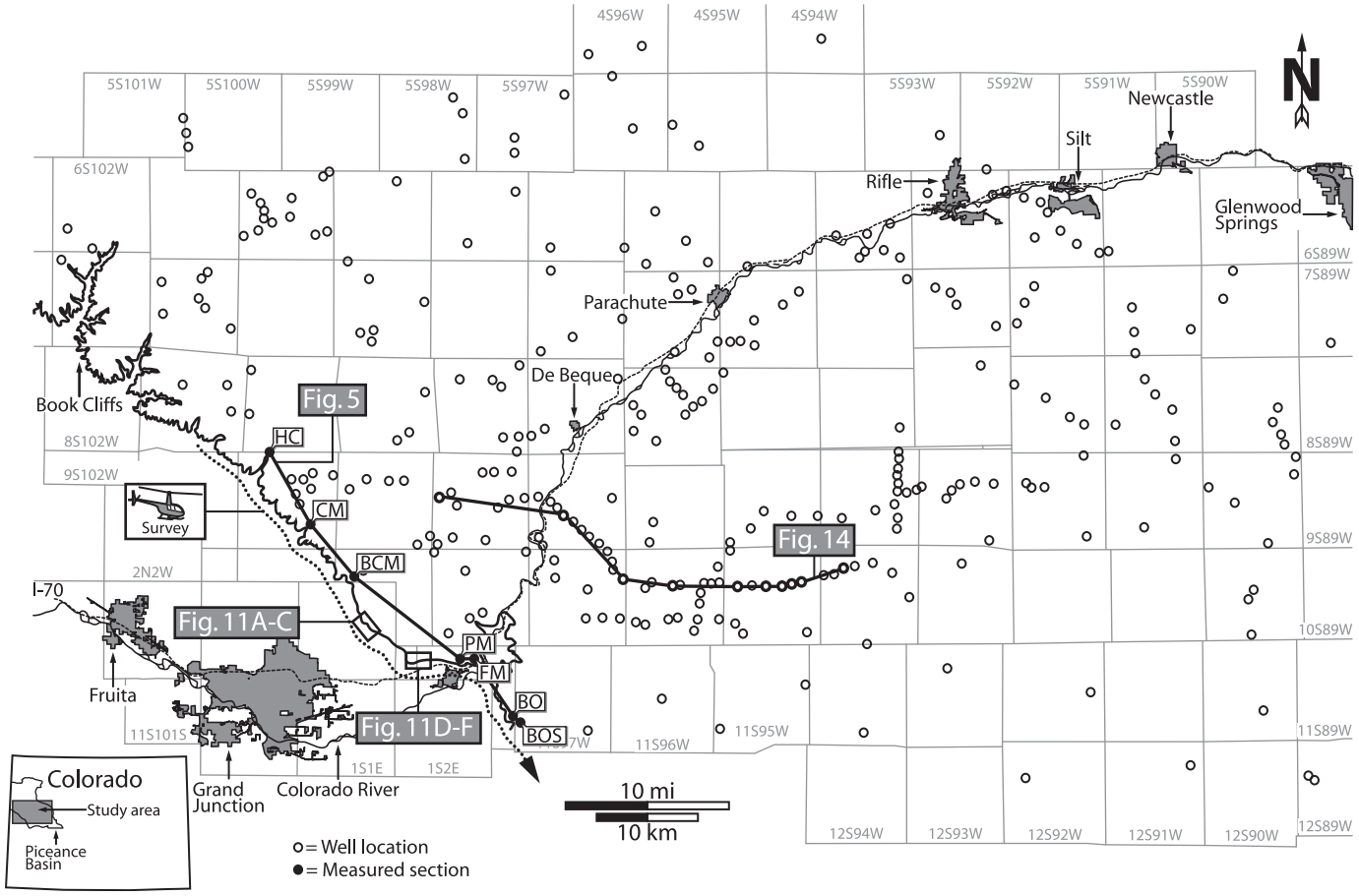

FIG. 2.—Map of study area, showing measured sections, well locations, and the position of Figures 5, 11 (A–C and D–F), and 14. Measured sections, from northwest to southeast, are abbreviated are as follows: HC, Hunter Canyon; CM, Corcoran Mine; BCM, Book Cliffs Mine; PM, Palisade Mine; FM, Farmers Mine; BO, Blowout; BOS, Blowout south. Note the delineation of townships and escarpment of Book Cliffs, as well as the southeast trajectory of the helicopter survey (dotted line).

Piceance basin has an asymmetric geometry in cross section, with gently dipping western and southwestern margins and a sharply upturned eastern flank (Johnson 1989). The western borders are thought to be underlain by west-dipping reverse faults, while the eastern margins are interpreted to be underlain by similar east-dipping structures (Gries 1983; Mederos et al. 2005). Similar reverse faults are considered to underlie three closed anticlines in the southeastern part of the basin: the Divide Creek and Wolf Creek structures (Fig. 3), and the Coal basin anticline (not illustrated). The Douglas Creek arch is thought to be a continuation of the Rock Springs uplift of southwestern Wyoming, from which it is now separated by the east-trending Uinta uplift of latest Cretaceous age (Mederos et al. 2005).

UPPER CAMPANIAN STRATIGRAPHY

Upper Campanian stratigraphy in the southern Piceance basin consists of approximately 168 m (550 ft) of nonmarine to shallow marine siliciclastic and coal-bearing strata assigned to the Mount Garfield Formation (Kirschbaum and Hettinger 2004). This unit is subdivided in ascending order into the Corcoran, Cozzette, and Rollins members (Fig. 4), all of which accumulated prior to the development of the present-day structural basin. The Cozzette Sandstone, named for the Cozzette mine north of the town of Palisade, Colorado (Young 1955), as well as the other members of the formation, is composed of sediment that was shed eastward via fluvial systems from the Sevier orogen (Young 1966; Franczyk 1989; Patterson et al. 2003). In the northern Piceance basin, the temporal equivalent of the Mount Garfield is largely nonmarine (Patterson et al. 2003), and is referred to as the Iles Formation. Additional nomenclatural details beyond the scope of this paper are discussed by Young (1955), Collins (1976), Franczyk (1989), Johnson (1989), Hettinger and Kirschbaum (2003), and Patterson et al. (2003).

DATA AND METHODOLGY

Seven sections, ranging from approximately 46 to 61 m (150 to 200 ft) in thickness and spanning a lateral distance of more than 37 km (23 miles), were initially measured and described in the Cozzette Sandstone along the eastern Book Cliffs during 2002–2003 (HC to BOS in Fig. 2). While the attempt to trace surfaces with binoculars contributed significantly to our preliminary interpretation (Madof 2006; Kamola et al. 2007), rugged topography and inaccessible canyons left several critical issues unresolved. Following a field trip organized for the Geological Society of America in October 2007 (Kamola et al. 2007), it was therefore decided to expand the original outcrop study with a high-resolution photographic survey of the eastern Book Cliffs by helicopter in August 2008, and by making use of publicly available well logs obtained from the Colorado Oil and Gas Commission.

The aerial survey, which consisted of digital videos and more than 1,500 overlapping photographs, involved two flights for 40 km (24.9 mi) along the cliffs, at the same elevation and within a few hundred lateral meters of it. The survey allowed surfaces and stratal units to be physically traced on photographs and digital video, and thus the correlation of

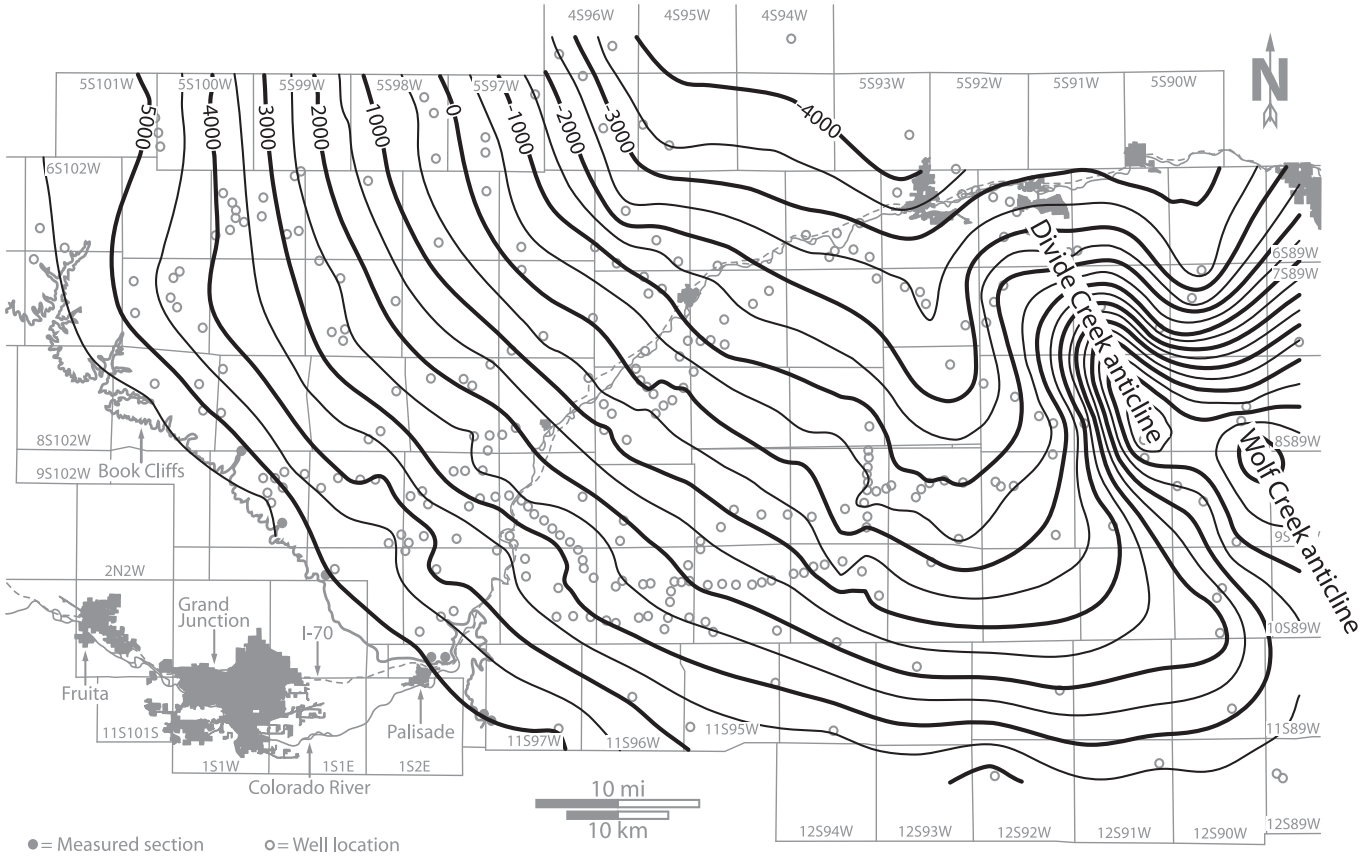

FIG. 3.—Structure contour map for top of Cozzette Sandstone in southern Piceance basin, showing inclination towards the northeast. The Divide Creek and Wolf Creek anticlines are among the most productive gas fields in the Piceance basin (Johnson 1989). Contour interval is 500 ft (152 m).

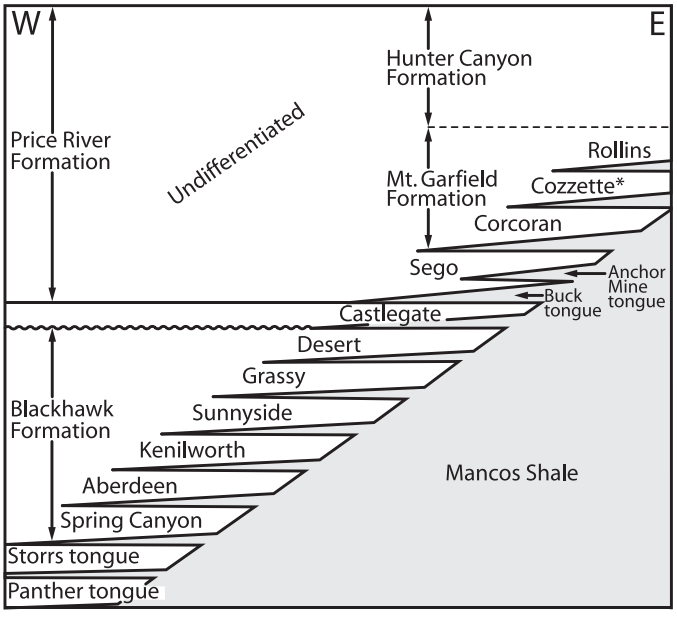

FIG. 4.—Chart of generalized Late Cretaceous stratigraphy exposed in the Book Cliffs of eastern Utah and western Colorado (modified from Young 1955). Note that the Price River Formation (eastern Utah) is laterally equivalent to the Hunter Canyon and Mount Garfield formations (western Colorado). The Cozzette Sandstone (star) overlies the Corcoran and underlies the Rollins.

measured sections. The subsurface dataset consists of downhole logs for 294 wells, organized in a series of cross sections with a spacing that ranges from 0.6 to 16.6 km (0.4 to 10.3 mi) and averages less than a few kilometers. Wells closest to the outcrop are within 1.0–6.4 km (0.6–4.0 mi) of measured sections. The top of the Cozzette, which is associated with a regional shale interval in outcrop (the base of the Rollins Sandstone Member) and positive gamma-ray and negative resistivity deflections in the subsurface, was used as a datum. Well-log correlations were constrained regionally at depth by a high gamma-ray response identified as the base of the Castlegate Sandstone (i.e., top of the Mancos Shale) by Patterson et al. (2003). (See Fig. 4 for stratigraphic position.)

The combination of outcrop, photographic, and well data used in this study cover approximately 10,960 km^2 (4,250 mi^2) in the southern Piceance basin (Figs. 1B, 2). Measured sections and their nearest neighbor wells provide a point of departure for the subsurface interpretation. Stratigraphic discontinuities (erosional surfaces, offlap surfaces more generally, and flooding surfaces), identified in outcrop, physically traced in photographs and digital videos, and projected into the subsurface, are the basis for a three-dimensional interpretation of stratal geometry.

PREVIOUS INTERPRETATIONS

Before this study, the Cozzette Sandstone was interpreted to consist of three sheet-like shallow marine parasequences, truncated by sequence boundaries located at the top of the first cycle, and overlying the member (Madof 2006; Kamola et al. 2007). This geometry was inferred to have been associated with north-trending paleoshoreline orientations, suggesting

TABLE 1.—*Twelve lithofacies composing the Cozzette Sandstone. All data were collected from measured sections.*

Lithofacies	Lithology	Sedimentary Structures	Bedding
(1) Bioturbated silty shale	Dark gray-blue to gray-brown silty shale	Bioturbation and millimeter-scale laminae	Tabular; intervals range from < 0.1 m to > 12.2 m
(2) Hummocky cross-stratified sandstone	Light brown, very fine- to fine-grained sandstone, with local rip-up clasts and mud drapes	Hummocky and swaly cross-stratification, with abundant *Ophiomorpha* and local *Cylindrichnus*	Tabular to lenticular; thicknesses range from < 0.1 m (individual beds) to > 9.8 m (amalgamated beds); beds exhibit coarsening-upward grain-size trend
(3) Trough cross-stratified sandstone	White to light brown, fine- to medium-grained sandstone, with intervals of rip-up clasts, mud, and carbonaceous drapes	Trough cross-stratification, with scattered *Ophiomorpha* and unidentified burrowing	Tabular, lenticular, and wedge; thicknesses range from < 0.1 m (individual beds) to > 5.7 m (amalgamated beds); beds exhibit coarsening, fining, or no upward grain-size trend
(4) Planar cross-stratified sandstone	Light brown, fine- to medium-grained sandstone, with local mud and carbonaceous drapes	Planar cross-stratification, with scattered *Ophiomorpha*	Tabular; thicknesses of individual beds range from 0.4 to 0.7 m; beds exhibit no upward grain-size trend
(5) Subparallel-laminated sandstone	Light brown, fine- to medium-grained sandstone, with local mud drapes	Subparallel laminae, with scattered *Ophiomorpha*	Tabular; thicknesses of individual beds range from 0.6 to 1.1 m; beds exhibit no upward grain-size trend
(6) Parallel-laminated sandstone	White to light brown, very fine- to medium-grained sandstone	Parallel laminae, with scattered *Ophiomorpha*	Tabular; thicknesses range from < 5 cm (individual beds) to > 3.1 m (amalgamated beds); beds exhibit coarsening or no upward grain-size trend
(7) Coal	Vitreous black coal, with sparse amber nodules	Coal veins, ranging in thickness from < 1 cm to > 2 cm	Coal seams range in thickness from < 0.1 m to > 0.4 m
(8) Wave-rippled sandstone	Light brown, very fine-grained sandstone, with intervals of mud and carbonaceous drapes	Wave-rippled sandstone, with local flasers, wavy, and lenticular bedding	Tabular to lenticular; thicknesses of individual beds range from < 1 cm to > 0.4 m; beds exhibit coarsening or no upward grain-size trend
(9) Current-rippled sandstone	Light brown, very fine- to medium-grained sandstone, with local mud and carbonaceous drapes	Current-rippled sandstone	Tabular to lenticular; thicknesses of individual beds range from < 2 cm to > 0.1 m; beds exhibit no upward grain-size trend
(10) Sigmoidal cross-stratified sandstone	Light brown, fine- to medium-grained sandstone, with local rip-up clasts and carbonaceous mud drapes	Sigmoidal cross-stratification	Tabular to lenticular; thicknesses of individual beds range from < 0.1 m to > 0.4 m; beds exhibit no upward grain-size trend
(11) Carbonaceous silty shale	Dark gray to black carbonaceous silty shale, with white silty laminae	Millimeter-scale laminae	Tabular; intervals range from < 0.1 m to > 3.9 m
(12) Burrowed sandstone	Gray to brown, fine- to medium-grained sandstone	Bioturbation	Tabular; thicknesses of individual beds range from 0.6–0.8 m; facies composed of individual bed (grain-size trend not applicable)

that the eastern Book Cliffs escarpment exposed an oblique-dip view of the Cozzette. The main difficulty with this interpretation, as well as those suggesting northeast paleoshoreline trends (Zapp and Cobban 1960; Warner 1964; Collins 1976; Johnson 1989, 2003; Franczyk 1989; Kennedy et al. 2000) is that shoreface cycles extend laterally for many kilometers (i.e., an exceedingly broad transition from foreshore to offshore settings), without a clear explanation of how coarse-grained sediments were transported in shallow marine environments. The proposed interpretation of the Cozzette Sandstone resolves these issues, draws particular attention to the significance of offlap, and concludes that Cozzette outcrops in western Colorado display an increasingly strike-oriented view up-section.

LITHOFACIES ASSEMBLAGES

The Cozzette Sandstone is divided into 12 lithofacies (Table 1) and 6 lithofacies assemblages (Table 2) on the basis of measured sections (Figs. 5, 6). Lithofacies are distinguished principally using lithology and sedimentary structures. Lithofacies assemblages are interpreted on the basis of successions of facies and vertical trends in grain size and bed thickness.

The six lithofacies assemblages are shoreface–foreshore–swamp, fluvial channel, delta mouth bar, tidal flat, organic-poor swamp and floodplain, and organic-rich swamp. Shoreface–foreshore–swamp deposits are the thickest, most voluminous, and laterally most continuous assemblage in the study area. Fluvial channel and delta mouth bar assemblages are thinner and less voluminous, and they exhibit more internal variability. Tidal flat and organic-poor swamp and floodplain deposits are relatively thick, but they are present only at the Hunter Canyon measured section (HC in Figs. 5, 6). Organic-rich swamp deposits, the thinnest assemblage, are distributed widely within the nonmarine strata.

Similar facies of shallow marine, marginal marine, and nonmarine origin have been well-documented in detail in outcrop in the Late Cretaceous foreland basin of Utah (i.e., San Rafael anticline (Edwards et al. 2005a), Uinta basin (Van Wagoner et al. 1990; Van Wagoner 1991a, 1991b, 1995; Ainsworth and Pattison 1994; Pattison 1995; Hampson 2000; Hampson et al. 2001; Hampson and Storms 2003; Storms and Hampson 2005), and Wasatch Plateau (Edwards et al. 2005b)), New Mexico (i.e., San Juan basin (Buillit et al. 2002; Ambrose and Ayers 2007; Sixsmith et al. 2008)), and Wyoming (i.e., Hatfield dome (Mellere and Steel 1995; Mellere 1996) and Powder River basin (Vakarelov and Bhattacharya 2009)).

Shoreface–Foreshore–Swamp

Observation.—Complete upward-coarsening shoreface–foreshore assemblages, along with the associated coastal-plain swamp (Table 2), consist of a locally erosional planar base overlain in ascending order by: burrowed sandstone; intervals of bioturbated silty shale (Fig. 7A); hummocky cross-stratified sandstone (Fig. 7B); parallel-laminated sandstone with dense *Ophiomorpha*; trough cross-stratified sandstone (Fig. 7C) with local planar cross-stratified sandstone; parallel- (Fig. 7D) or subparallel-laminated sandstone; and coal. Deposits in the assemblage range from approximately

TABLE 2.—*Six lithofacies assemblages that constitute the Cozzette. Table shows both outcrop (grain size) and subsurface (GR and R) expressions.*

Facies Assemblage	Vertical Facies Trends (in ascending order)	Vertical Grain-Size Trends; Log Response (GR, R)	Interpretation of Depositional Environment
(A) Shoreface–foreshore–swamp	Planar base overlain by (12) burrowed sandstone, (1) bioturbated silty shale, (2) hummocky cross-stratified sandstone, (6) parallel-laminated sandstone with dense *Ophiomorpha,* (3) trough cross-stratified sandstone with local (4) planar cross-stratified sandstone, (6) parallel-laminated or (5) subparallel-laminated sandstone, capped by (7) coal	Upward coarsening; upward decrease in GR; upward increase in R	Shoreface deposited in wave-dominated shallow marine environment [components of shoreface are interpreted as transgressive lag (12), offshore transition to distal lower shoreface (1), distal to proximal lower shoreface (2), middle shoreface (6), upper shoreface (3 and 4)], foreshore (5 and 6), and organic-rich swamp (7)
(B) Fluvial channel	Erosional base topped with rip-up clasts overlain by (3) trough cross-stratified sandstone, with local (8) wave-rippled sandstone, capped by unidentified burrowing or rooting	Upward fining; upward increase in GR; upward decrease in R	Fluvial systems (relatively straight to meandering and multi-channeled) deposited within incised valley
(C) Delta mouth bar	Planar to erosional base overlain by (11) carbonaceous silty shale, (8) wave-rippled or (9) current-rippled sandstone, and (6) parallel-laminated sandstone, capped by (7) coal, rooting, or burrowing (escape structures)	Upward coarsening; upward decrease in GR; upward increase in R	Deltas deposited within estuaries in incised valley and on coastlines (updip equivalent of shoreface)
(D) Tidal flat	Planar base overlain by (8) wave-rippled sandstone or (3) trough cross-stratified sandstone with local rip-up clasts, (5) subparallel-laminated sandstone, (10) sigmoidal cross-stratified sandstone, and (8) wave-rippled or (3) trough cross-stratified sandstone	Upward fining; upward increase in GR; upward decrease in R	Tidal flat deposited within estuary or coastline (updip equivalent of shoreface)
(E) Organic-poor swamp and floodplain	(11) Carbonaceous silty shale with minor (7) coal	No trend	Organic-poor swamp and floodplain deposited within estuary or coastline (updip equivalent of shoreface)
(F) Organic-rich swamp	(7) Coal seams with locally interstratified (11) carbonaceous silty shale	No trend	Organic-rich swamp deposited within estuaries in incised valley and on coastline

7 to 35 m (23 to 115 ft) in thickness and extend laterally in outcrop for more than ~ 28.5 km (17.7 mi). Incomplete assemblages are missing at least one lithofacies from the top and/or base of the deposit.

Interpretation.—Sediments of the shoreface–foreshore–swamp assemblage are interpreted to represent progradation in a wave-dominated shallow marine environment (cf. Van Wagoner et al. 1990). Where present, basal burrowed sandstone is interpreted as a transgressive lag, and overlying bioturbated silty shale is inferred to have accumulated in the offshore transition to distal lower shoreface. Hummocky cross-stratified sandstone is interpreted to have been generated by storm-induced oscillatory combined flow, characteristic of the distal to proximal lower shoreface (Dott and Bourgeois 1982; Walker and Plint 1992; Ito et al. 2001). Parallel-laminated sandstone with dense *Ophiomorpha* is interpreted to have accumulated in the build-up to surf-zone regions of the middle shoreface (Reinson 1984). Trough cross-stratified sandstone and parallel- to subparallel-laminated sandstone represents the surf zone of the upper shoreface, and swash zone of the foreshore, respectively (Clifton et al. 1971). Coal signifies compaction and induration of plant remains in a swamp environment, overlying shallow marine deposits.

Fluvial Channel

Observation.—Complete upward-fining fluvial channel assemblages (Table 2) exhibit an erosional base (Fig. 8A) overlain in ascending order by: rip-up clasts; trough cross-stratified sandstone (Fig. 8B) with local wave-rippled sandstone (Fig. 8C); and the presence of burrows or roots (Fig. 8D). Deposits in the assemblage range from approximately 4.5 to 7.3 m (15 to 24 ft) in thickness and extend laterally in outcrop for as much as ~ 1.4 km (0.9 mi). Accumulations exhibit the local development of inclined heterolithic stratification (cf. Thomas et al. 1987). Incomplete assemblages are missing at least one lithofacies from the top of the deposit.

Interpretation.—The fluvial-channel facies assemblage is interpreted to have been deposited in relatively straight (downstream accreting) to meandering (laterally accreting) multi-channel river systems. The interpretation is based on the presence of multiple channelized upward-fining deposits at the same stratigraphic level, and of both even parallel and inclined stratification in three dimensions. Because the bulk of the fluvial facies (channel belts) were observed during the helicopter survey of the Cozzette, and not by direct inspection, it was not possible to identify rooting and/or coal at the tops of individual successions.

Delta Mouth Bar

Observation.—Complete upward-coarsening delta-mouth-bar assemblages (Table 2; Fig. 9A) consist of a planar to erosional surface overlain in ascending order by either: carbonaceous silty shale; wave- or current-rippled sandstone; parallel-laminated sandstone (Fig. 9B); and coal, roots, burrows, or escape structures. Deposits in the assemblage range

→

FIG. 5.—Proposed sequence stratigraphic interpretation of the Cozzette Sandstone. Measured sections were correlated from digital video and continuous photographs obtained during a helicopter survey of the member (see Fig. 2 for helicopter route). The stratigraphic positions of the ammonites *Didymoceras nebrascense* and *Didymoceras stevensoni*, as well as *Exiteloceras jenneyi*, are superimposed onto closest measured sections to where they were identified by Gill and Hail (1975) and Madden (1989), respectively. Camera icons situated at the top of measured sections identify Figures 12A–H. Note the location of Figure 11A to C southeast of BCM, and Figure 11D–F northwest of PM. See Figure 2 for measured section abbreviations. Circled numbers 1–4 and 6 denote shallow marine to marginal marine parasequences; IVF1 and IVF2 specifies incised-valley fill; SB1 and SB2 refer to sequence boundaries (erosional); FS indicates a flooding surface; and LA signifies lateral accretion. Abbreviations at the base of measured sections for mean grain sizes are as follows: m, mud; s, silt; vfl, very fine lower sand; vfu, very fine upper sand; fl, fine lower sand; fu, fine upper sand; ml, medium lower sand. Note that an alternative interpretation identifies SB1 as the only erosional sequence boundary in the Cozzette Sandstone, placing overlying fluvial and estuarine deposits into a single composite incised-valley fill. In this scenario, SB2 would be interpreted as a large-scale internal scour surface.

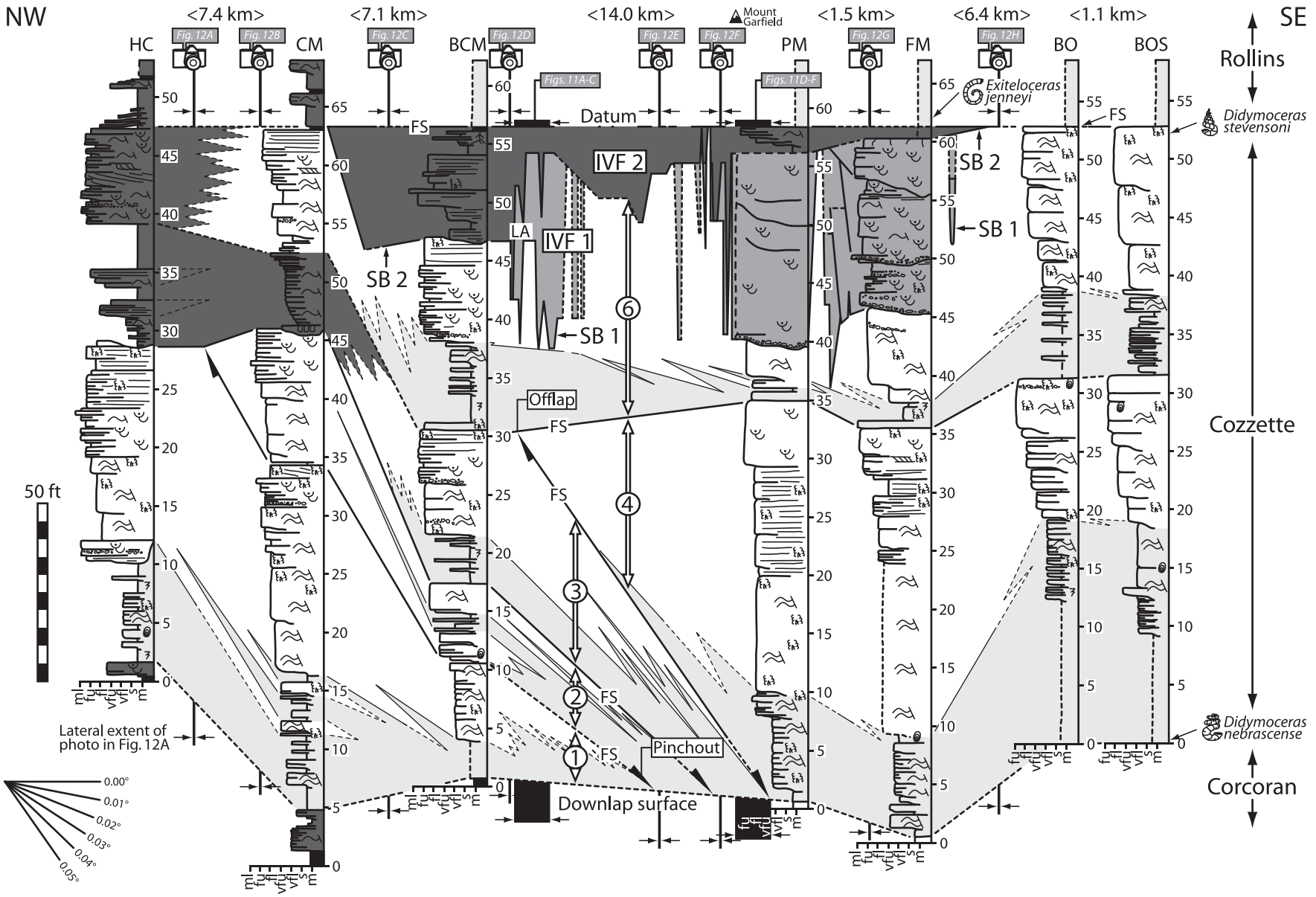

Cross section symbols

- = Current ripples
- = Hummocky cross-stratification
- = Subparallel laminae
- = Parallel laminae
- = Planar cross-stratification
- = Rip-up clasts
- = Sigmoidal cross-stratification
- = Trough cross-stratification
- = Wave ripples
- = Burrowing
- = Coal
- = *Cylindrichnus*
- = *Glossifungites*
- = *Ophiomorpha*
- = Unidentified burrows
- = Rooting

Depositional environments

- = Shoreface-foreshore-swamp
- = Fluvial
- = Estuarine

Ammonite ages

- = 75.05-74.28 Ma
- = 75.74-75.05 Ma
- = 76.38-75.74 Ma

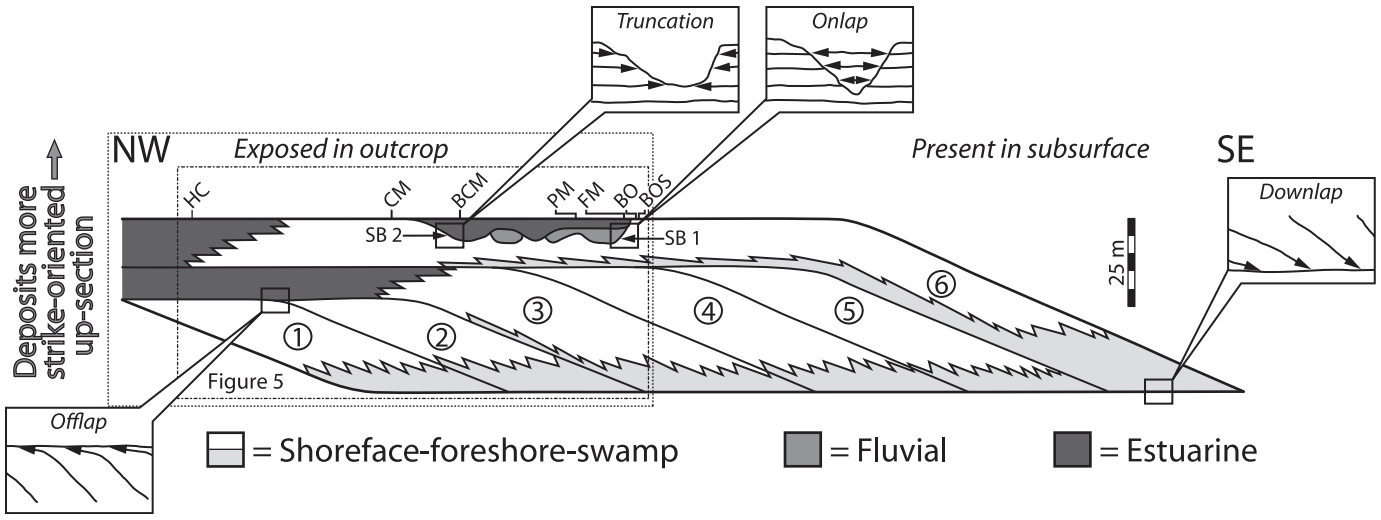

FIG. 6.—Simplified schematic cross section of Cozzette Sandstone in southern Piceance basin, showing wedge-shaped shoreface–foreshore–swamp parasequences and overlying incised-valley fills. The stratigraphic architecture is defined geometrically by the presence of offlap, truncation, onlap, and downlap. Parasequences become more strike-oriented up-section. Note the position of Figure 5 (exposed in outcrop) to the northwest, as well as its subsurface equivalent to the southeast.

from approximately 2.1 to 4.6 m (7 to 15 ft) in thickness and extend laterally in outcrop for at least ~ 6.4 km (4.0 mi). Incomplete assemblages are missing at least one lithofacies from the top and/or base of the deposit.

Interpretation.—Sediments of the delta-mouth-bar assemblage are interpreted to represent progradation into or at a wave-influenced estuary or coastline. The upward-coarsening character of the assemblage (i.e., a vertical transition from carbonaceous silty shale,

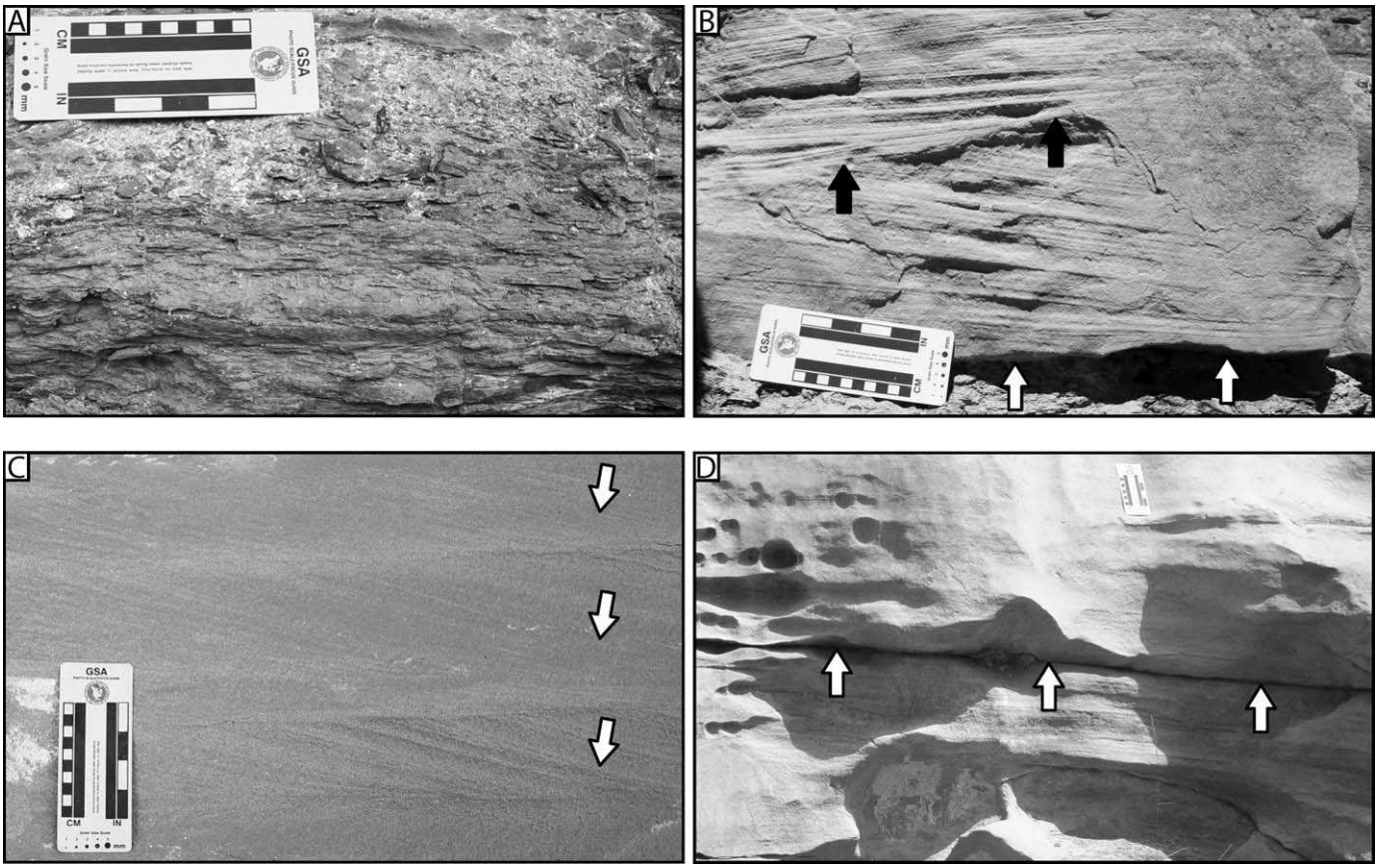

FIG. 7.—Shoreface and foreshore deposits (modified from Madof 2006). **A)** Bioturbated silty shale. **B)** Hummocky cross-stratification, showing erosional base (white arrows) and low-angle truncation surface (black arrows). **C)** Trough cross-stratification. White arrows identify cross beds. **D)** Sandstone beds consisting of parallel laminae, separated by silty shale interval (white arrows).

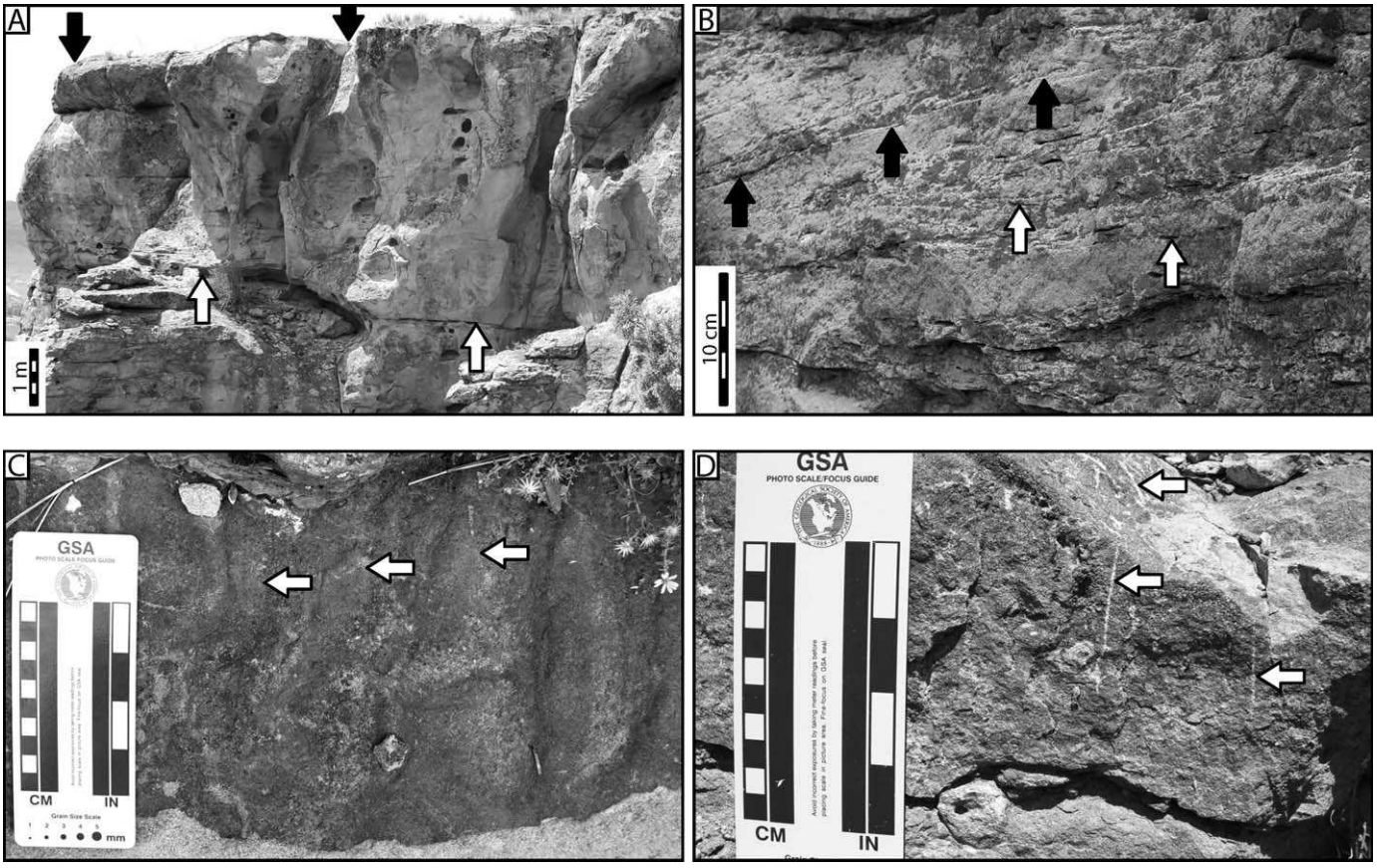

FIG. 8.—Fluvial channel deposits. **A)** Channel fill exhibits scoured base (white arrows) and relatively flat top (black arrows). Maximum thickness is approximately 5.5 m (18 ft) (modified from Madof 2006). **B)** Trough cross-stratification, showing cross beds draped with carbonaceous mud (black arrows) and rip-up clasts (white arrows). **C)** Current ripples (in plan view), displaying relatively uniform crest trend (white arrows). **D)** Rooting or unidentified burrowing (white arrows) in burrowed sandstone facies (modified from Madof 2006).

to wave-rippled and current-rippled sandstone, to parallel-laminated sandstone) is consistent with shoaling in an increasingly high-energy marginal marine to shallow marine depositional environment. Where present, rooting and/or coal suggest accumulation at or above sea level.

Tidal Flat

Observation.—Complete upward-fining tidal-flat assemblages (Table 2; Fig. 10A) consist of a planar surface overlain in ascending order by: wave-rippled or trough cross-stratified sandstone with locally derived

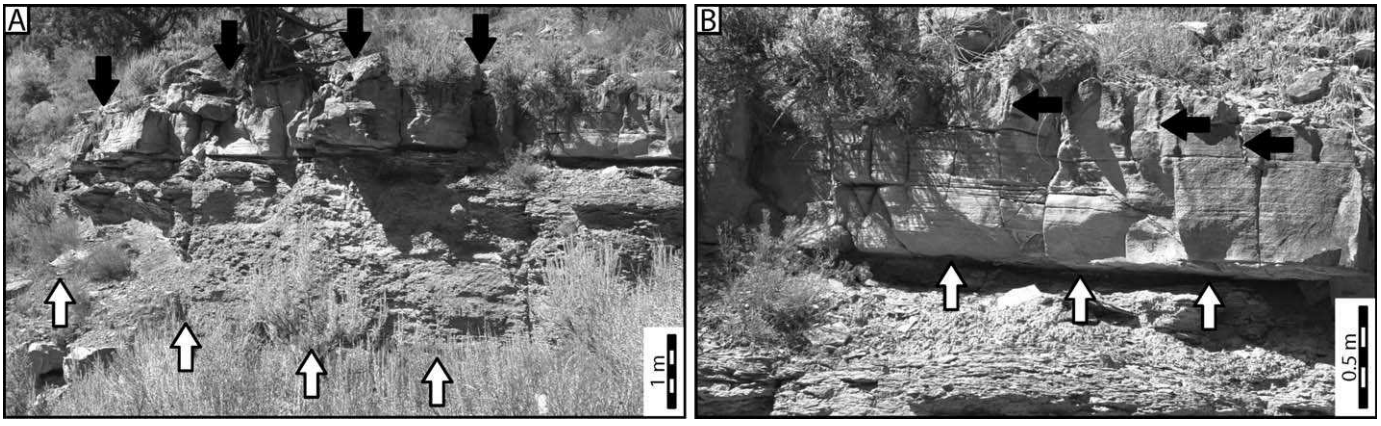

FIG. 9.—Delta-mouth-bar deposits. **A)** Accumulation displays flat-based siltstone (white arrows) erosionally overlain by sandstone bed with relatively flat top (black arrows). Maximum thickness is approximately 4 m (13 ft). **B)** Parallel laminae located at top of deposit, showing locally erosional base (white arrows) and *Ophiomorpha* burrowing (black arrows).

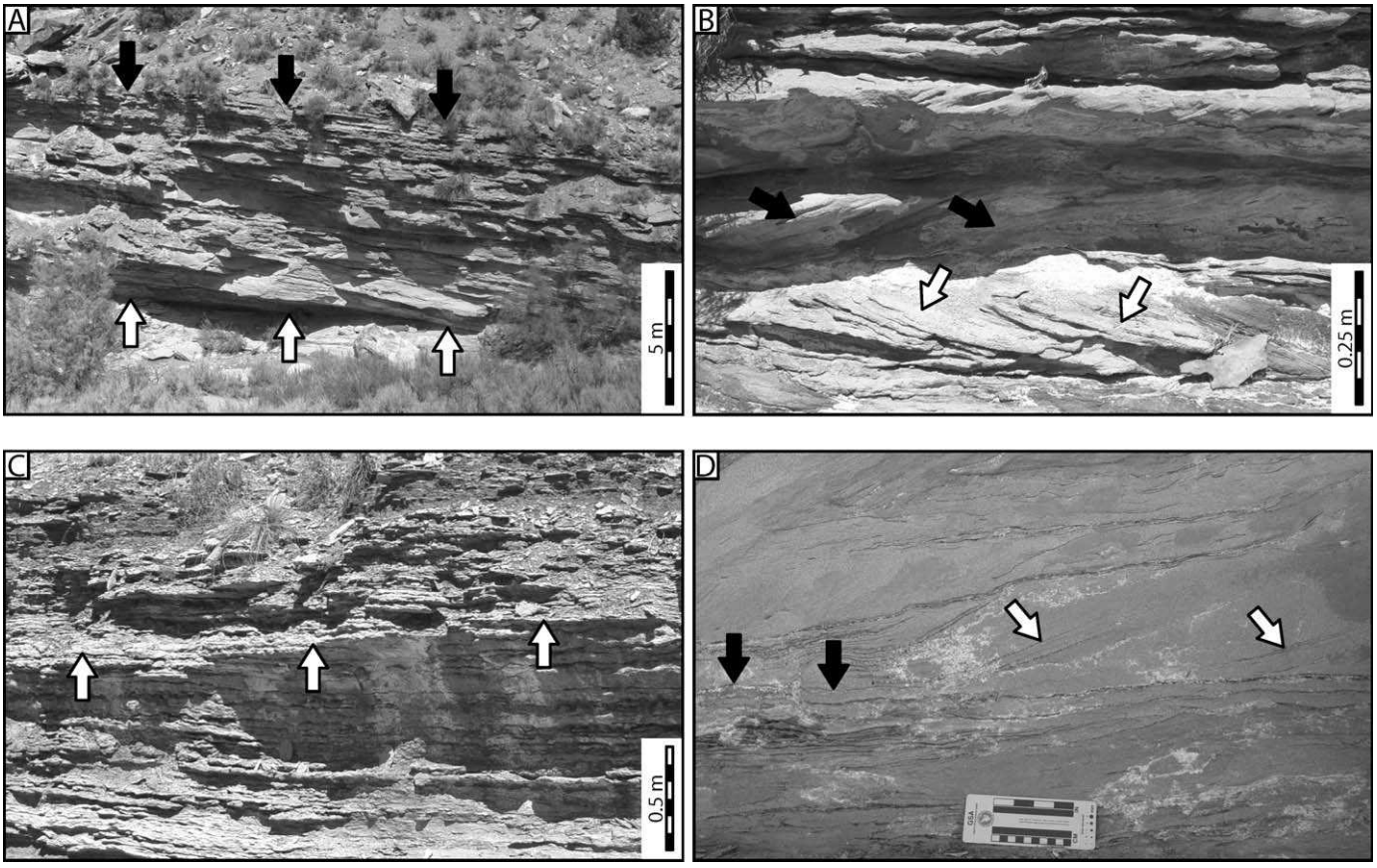

FIG. 10.—Tidal-flat deposits. **A)** Accumulation displays planar base (white arrows) and flat top (black arrows). **B)** Sigmoidal cross-stratification, showing opposing cross-bed dips (herringbone cross-stratification white and black arrows). (Modified from Madof 2006.) **C)** Wavy bedding (below white arrows) abruptly overlain by lenticular bedding (above white arrows). **D)** Compound-complex bedding, consisting of trough cross-stratification (white arrows identify cross beds) laterally grading into low amplitude wave ripples (black arrows; modified from Madof 2006.)

rip-up clasts; subparallel-laminated sandstone; sigmoidal cross-stratified sandstone (Fig. 10B); and wave-rippled (flaser, wavy, and lenticular bedding; Fig. 10C) or trough cross-stratified sandstone (Fig. 10D). The assemblage is approximately 9.1 m (30 ft) in thickness and extends laterally in outcrop for as much as ~ 3.2 km (2.0 mi).

Interpretation.—Tidal-flat sediments are interpreted to represent deposition in or at a tide-influenced estuary or coastline. The upward-fining character of the assemblage (i.e., a vertical transition from sigmoidal, to flaser, to wavy, to lenticular bedding) suggests shoaling in a muddy intertidal zone (Reineck and Singh 1980).

Organic-Poor Swamp and Floodplain

Observation.—The organic-poor swamp and floodplain assemblage consists of carbonaceous silty shale interbedded with minor coal. The assemblage is approximately 3.8 m (12.5 ft) in thickness and extends laterally in outcrop for as much as ~ 1.6 km (1.0 mi).

Interpretation.—Organic-poor swamp and floodplain sediments are interpreted to have accumulated in or at a wave- or tidally-influenced estuary or coastline. This interpretation is based on stratigraphic position between underlying wave-influenced deltaic deposits and overlying tidal-flat strata. The presence of carbonaceous silty shale, as well as minor interbedded coal, suggests suspension deposition in a low-lying poorly drained area. The lack of prominent root traces and coal at the top of the deposit suggests that the water was commonly too deep for rooting, or that the swamp and floodplain was not heavily vegetated for other reasons.

Organic-Rich Swamp

Observation.—The organic-rich-swamp assemblage consists of coal seams with locally interstratified carbonaceous silty shale and amber nodules. Deposits in the assemblage range from approximately 0.6 to 0.8 m (2 to 2.5 ft) in thickness and extend laterally in outcrop for up to several hundred meters.

Interpretation.—Organic-rich-swamp deposits are interpreted to have formed in response to compaction and induration of plant remains in subtropical to warm-temperate swamps (Collins 1976) with low siliciclastic input. Amber nodules indicate the presence of conifers. Organic-rich swamps are thought to have been located close to wave- or tide-influenced coastlines, or in estuaries.

STRATIGRAPHIC ARCHITECTURE

The Cozzette Sandstone consists of six offlapping shallow marine parasequences overlain by fluvial and estuarine deposits (Figs. 5, 6, 11; Table 3). This interpretation is based on the physical tracing of surfaces on continuous outcrop photographs and digital video obtained during the helicopter survey of the member (Figs. 11, 12; see Data and Methodology

TABLE 3.—*Stratigraphic architecture of the Cozzette Sandstone. Abbreviations are as follows: O = outcrop; S = subsurface. Average gradients were calculated from the compacted isopach maps of each parasequence (Figs. 13A–D).*

Unit	Depositional Environment	Geometry	Presence	Thinning Direction	Thickness	Extent	Gradient
Parasequence No. 1	Shoreface and swamp	Wedge-shaped (pinch out by downlap between BCM and PM)	O and S	Southeast	O: 0–27.4 m (0–90 ft) S: 0–29 m (95 ft)	O: ~ 21.7 km (13.5 mi) S: > 72 km (45 mi)	0.03°–0.04°
Parasequence No. 2	Shoreface	Wedge-shaped (pinch out by downlap between BCM and PM)	O and S	South to southeast	O: 0–11.7 m (0–38.5 ft) S: 0–19.8 m (64.9 ft)	O: ~ 14.2 km (8.8 mi) S: > 64 km (40 mi)	0.03°–0.06°
Parasequence No. 3	Marginal marine to shoreface, foreshore, and swamp	Wedge-shaped (pinch out by downlap NW of PM)	O and S	South	O: 0–18.3 m (0–60 ft) S: 0–34.8 m (114.2 ft)	O: ~ 28.5 km (17.7 mi) S: > 80 km (50 mi)	0.02°–0.07°
Parasequence No. 4	Shoreface	Wedge-shaped	O and S	South	O: 0–35 m (0–115 ft) S: 0–68 m (20.7 ft)	O: ~ 20.9 km (13 mi) S: ~ 56.3 km (35 mi)	0.05°–0.06°
Parasequence No. 5	Shoreface	Wedge-shaped	S	South	S: 0–22.5 m (79.5 ft)	S: > 24.1 km (15 mi)	0.03°–0.05°
Parasequence No. 6	Shoreface, foreshore, and swamp	Truncated wedge-shaped	S	South	O: 16.3–21.6 m (53.5–71 ft) S: > 19.2 m (62.9 ft)	S: > 32 km (51.5 mi)	
Incised valley fill No. 1	Fluvial	Truncated valley-shaped	O and S	Southeast and northwest	O: 0–20 m (0–67 ft) S: 0–19.5 m (0–63.9 ft)	S: > 24.1 km (15 mi) (width) > 72.4 km (45 mi) (length)	
Incised valley fill No. 2	Estuarine	Valley-shaped	O and S	Southeast and northwest	O: 0–10 m (0–32 ft) S: 0–14.6 m (0–47.9 ft)	S: > 53 km (33 mi) (width) > 72.4 km (45 mi) (length)	

section for details). Parasequences nos. 1 and 2, as well as nos. 3–5, constitute two distinct parasequence sets, with similar forestepping stacking patterns (Figs. 5, 6; terminology from Christie-Blick and Driscoll 1995). Parasequence no. 6, the youngest, is erosionally truncated by surfaces belonging either to two distinct incised-valley fills, or one composite fill.

Contour maps of compacted stratigraphic thicknesses (isopach maps) were created from available subsurface data. Thicknesses were not decompacted for this purpose, to preserve the integrity of first-order observations. Parasequences were flattened on the underlying downlap surface and were measured to their respective flooding surfaces. Incised-valley-fill deposits were flattened on the overlying base Rollins and were measured to their underlying sequence boundaries (or scour surfaces). A correction for structural inclination (i.e., postdepositional tilt) of the southern Piceance basin (Fig. 3) was made for each map by multiplying the interval thickness in each well by the cosine of the structural gradient. No correction is needed for well deviation because each well was drilled close to vertical.

Shallow Marine Parasequences

Each parasequence consists of wedge-shaped shoreface deposits, with isopachs of successive units revealing a change in the direction of thinning from southeast to south (Fig. 13; Table 3). At their updip pinchout, parasequences nos. 2 and 4–5 show marked offlap (Figs. 5, 11A–C, 14, 15) and a proximal geometric break in slope (i.e., rollover in Fig. 15). Our term "rollover," which is equivalent to the "depositional-shoreline break" of Van Wagoner et al. (1988), is used here in a descriptive sense (Pekar et al. 2003). Figure 16 shows the clinoform rollover positions with respect to time for parasequences nos. 1–5. The deposits progressively step out into the basin (i.e., southeast), deflect eastward, and become increasingly irregular.

Parasequences pinch out basinward by downlap, geometry that can be seen in outcrop for parasequences nos. 1–3 (between BCM and PM in Fig. 5; Fig. 11D–F) and in the subsurface for parasequence no. 1 (e.g., between wells Horseshoe Canyon #1-21 and USA #2-12 in Fig. 14). The same geometry is also expressed in map view in Figure 13. Gradients for flooding surfaces, which were calculated from the arctangent of slopes measured in Figure 13A–E, range from 0.02 to 0.07° (Table 3). Although this estimate is an underestimate, because decompaction would result in an increase in dip, inclinations are generally less than estimated for comparable surfaces in the Kennilworth Member of the underlying Blackhawk Formation, eastern Utah (Hampson 2000; see Fig. 4 for stratigraphic position).

Fluvial and Estuarine Incised-Valley Fills

Parasequence no. 6, the uppermost shallow marine interval in the Cozzette, is overlain in ascending order by both fluvial and estuarine deposits (Figs. 5, 6, 11, 17, and 18), and by shallow marine deposits of the Rollins Sandstone. Both fluvial and estuarine deposits rest with unconformable contact on shallow marine accumulations, with the northwest margin of fluvial accumulations (incised-valley fill no. 1) erosionally truncated beneath estuarine deposits (incised-valley fill no. 2). The erosional surfaces are interpreted as laterally persistent because available resolution is insufficient to recognize more complex geometry.

CLINOFORM ROLLOVER TRAJECTORY AND STACKING PATTERNS

Conventional wisdom suggests that parasequence stacking patterns can be deciphered geometrically by mapping shoreline or shelf-margin trajectories through time (Helland-Hansen and Martinsen 1996; Henriksen et al. 2011; Helland-Hansen et al. 2012). This concept is usually based on a single, vertically exaggerated, dip-oriented cross section, and serves

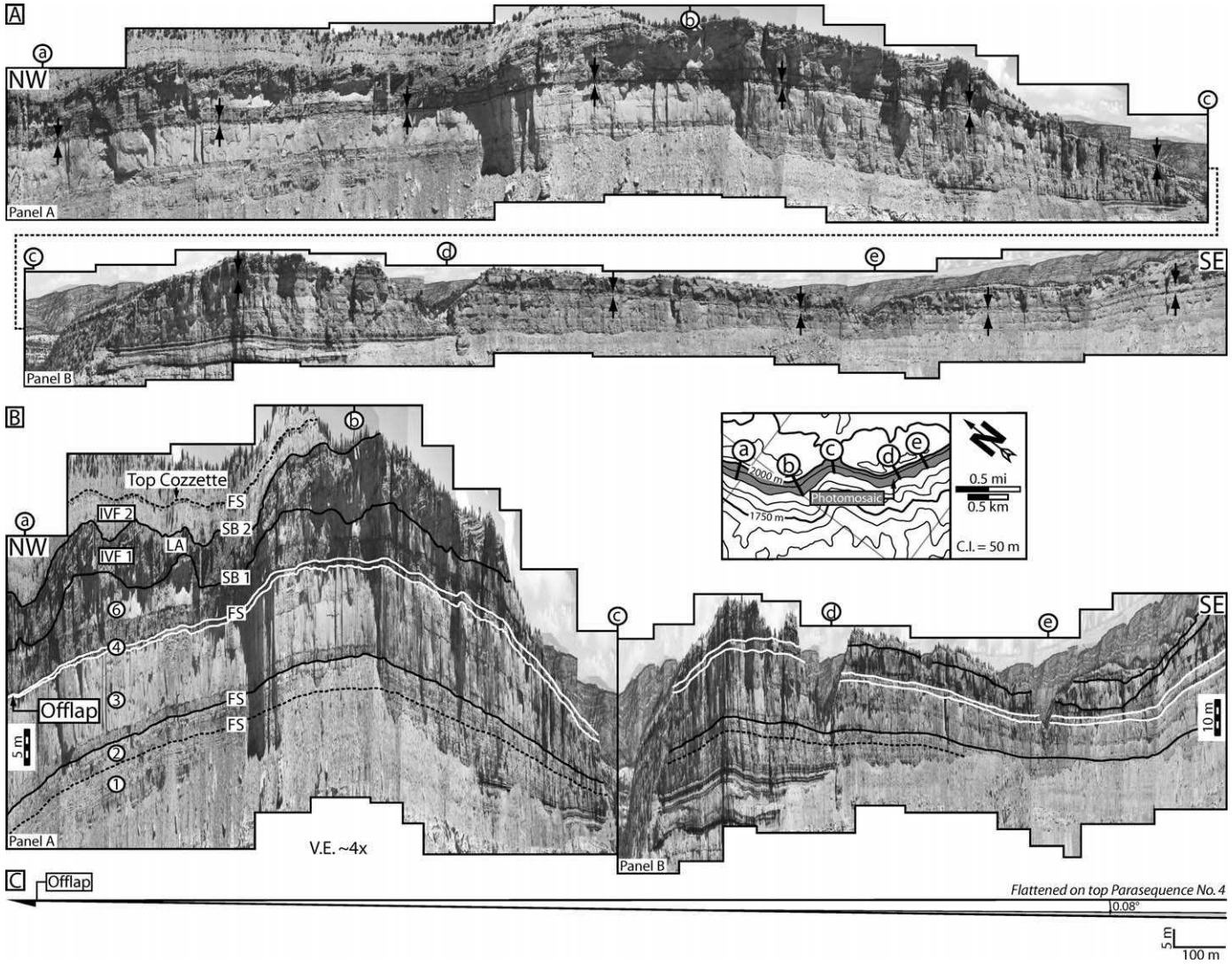

FIG. 11.—Photomosaics displaying outcrop expression of offlap and pinchout by downlap for the Cozzette Sandstone. A–C) Offlap exposed to the southeast of the BCM measured section. See Figure 2 for location. **A)** Panorama (uninterpreted) showing laterally extensive and flat-lying character of the Cozzette. Note that photographs are continuous and dotted line ties Panel A to B. Arrows delineate offlapping parasequence no. 4. **B)** Interpreted photographs from Part A, delineating parasequences nos. 1–4 and 6, as well as two overlying incised-valley fills. Note that offlapping parasequence no. 4 (white lines) grades from zero thickness in the northwest (left) to approximately 4 m in the southeast (right), a lateral distance of 2.8 km. See location map inset for tie points a to e. V.E., vertical exaggeration. See Figure 5 for abbreviations. **C)** Line drawing of parasequence no. 4 (from B) flattened on top flooding surface, illustrating the subtle thickening nature of the deposit. The 0.08° gradient was measured from the arctangent of the slope (i.e., thickness change of 4 m over a 2.8 km lateral distance) and is a compacted sediment thickness, oriented oblique to depositional dip.

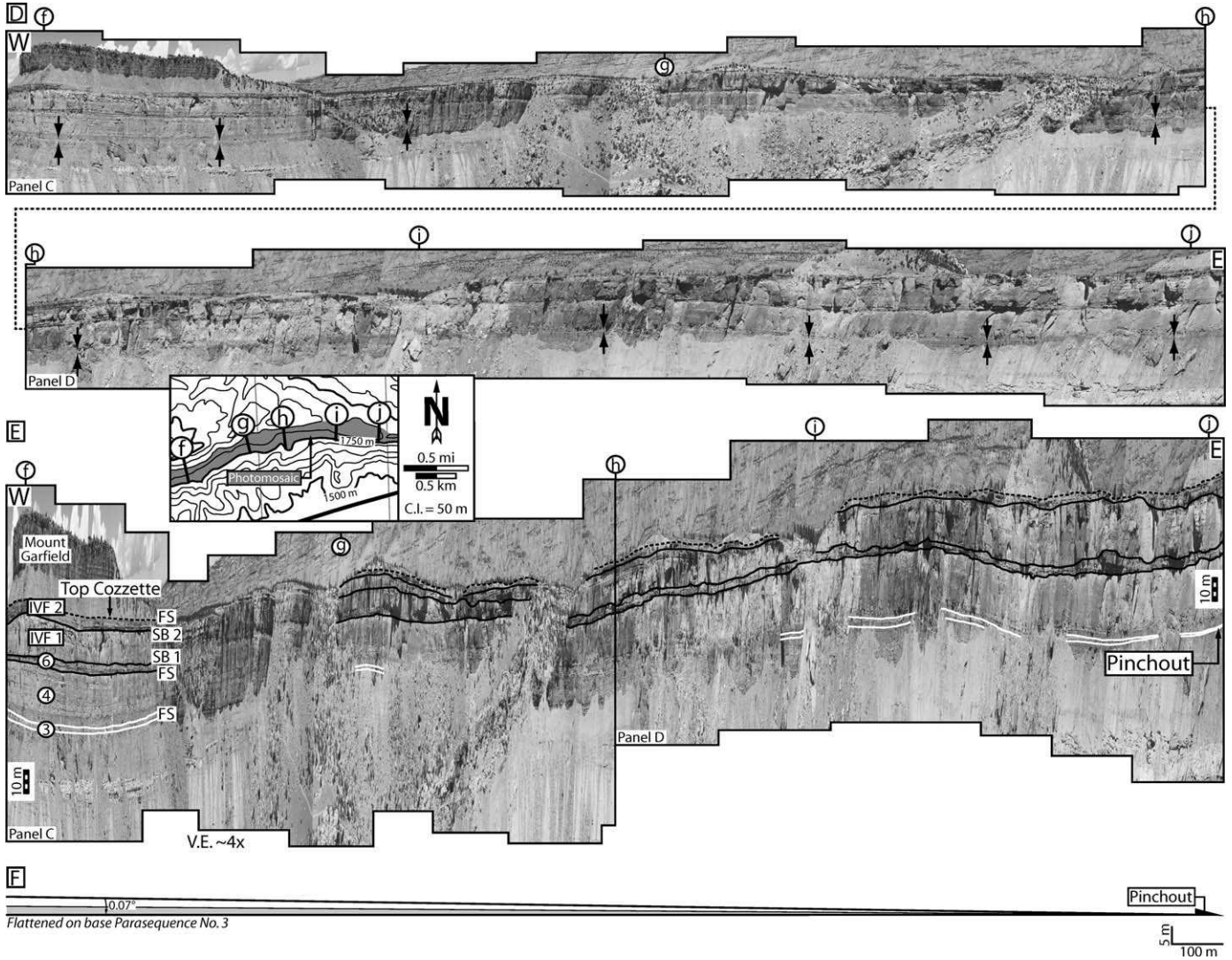

FIG. 11.—Continued. D–F) Pinchout by downlap exposed to the northwest of the PM measured section. See Figure 2 for location. **D)** Panorama (uninterpreted) showing laterally extensive and flat-lying character of the Cozzette. Note that photographs are continuous and dotted line ties Panel C to D. Arrows delineate downlapping parasequence no. 3. **E)** Interpreted photographs from Part D, delineating parasequences nos. 3–4, and 6, as well as two overlying incised-valley fills. Note that parasequence no. 3 (white lines) grades from less than 4 m in thickness towards the west (left) to approximately zero thickness towards the east (right), a lateral distance of 2.8 km. See location map inset for tie points f to j. V.E., vertical exaggeration. See Figure 5 for abbreviations. **F)** Line drawing of parasequence no. 3 (from E) flattened on bottom downlap surface, illustrating the subtle thinning nature of the deposit. The 0.07° gradient was measured from the arctangent of the slope (e.g., a thickness change of 3.8 m over a 2.8 km lateral distance) and is a compacted sediment thickness, oriented oblique to depositional dip.

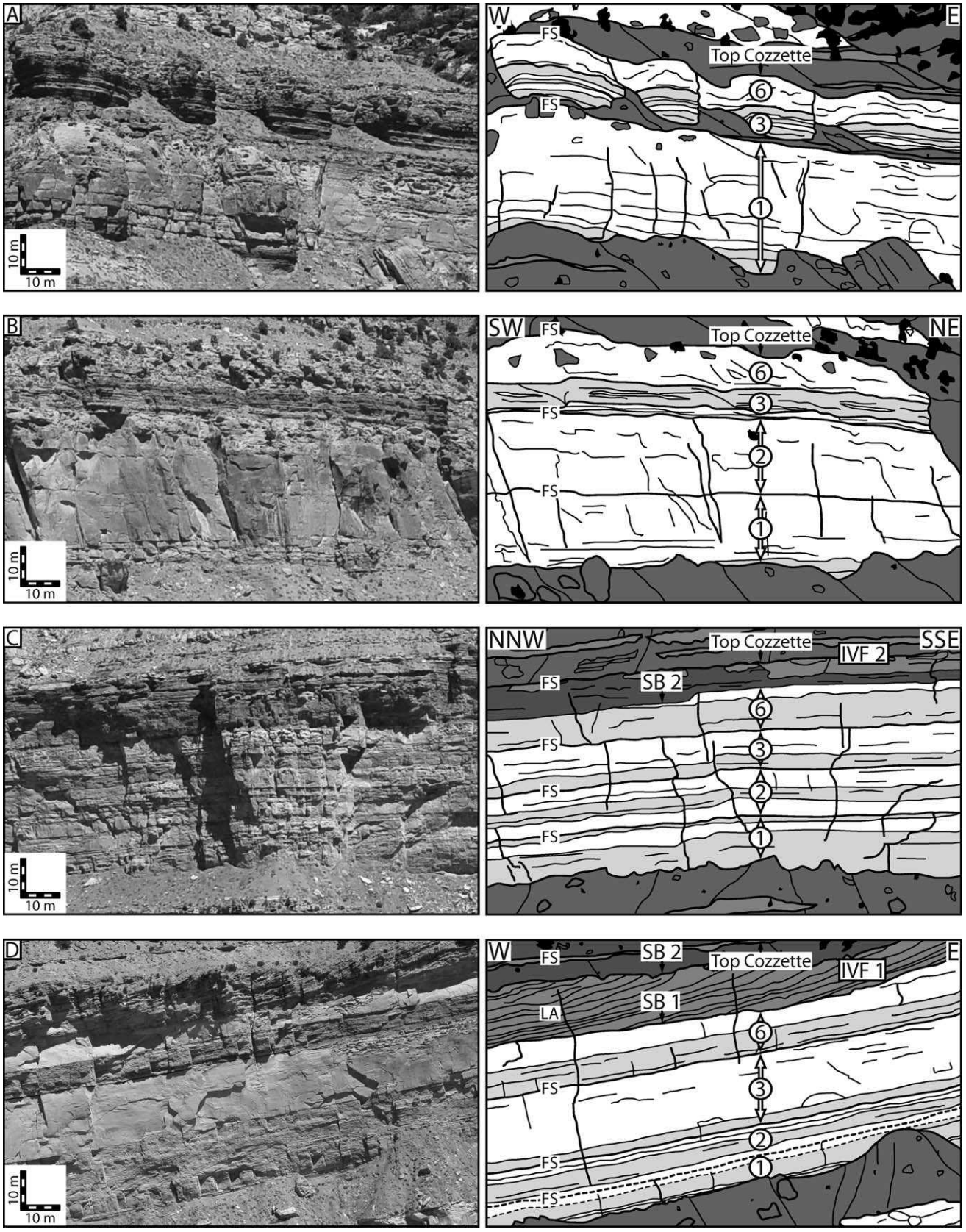

FIG. 12.—Photographs (uninterpreted, left and interpreted, right) showing outcrop expression of the Cozzette Sandstone. See Figure 5 for location of photographs (camera icon) relative to measured sections. Abbreviations and color scheme of interpreted depositional environments are the same as used in Figure 5.

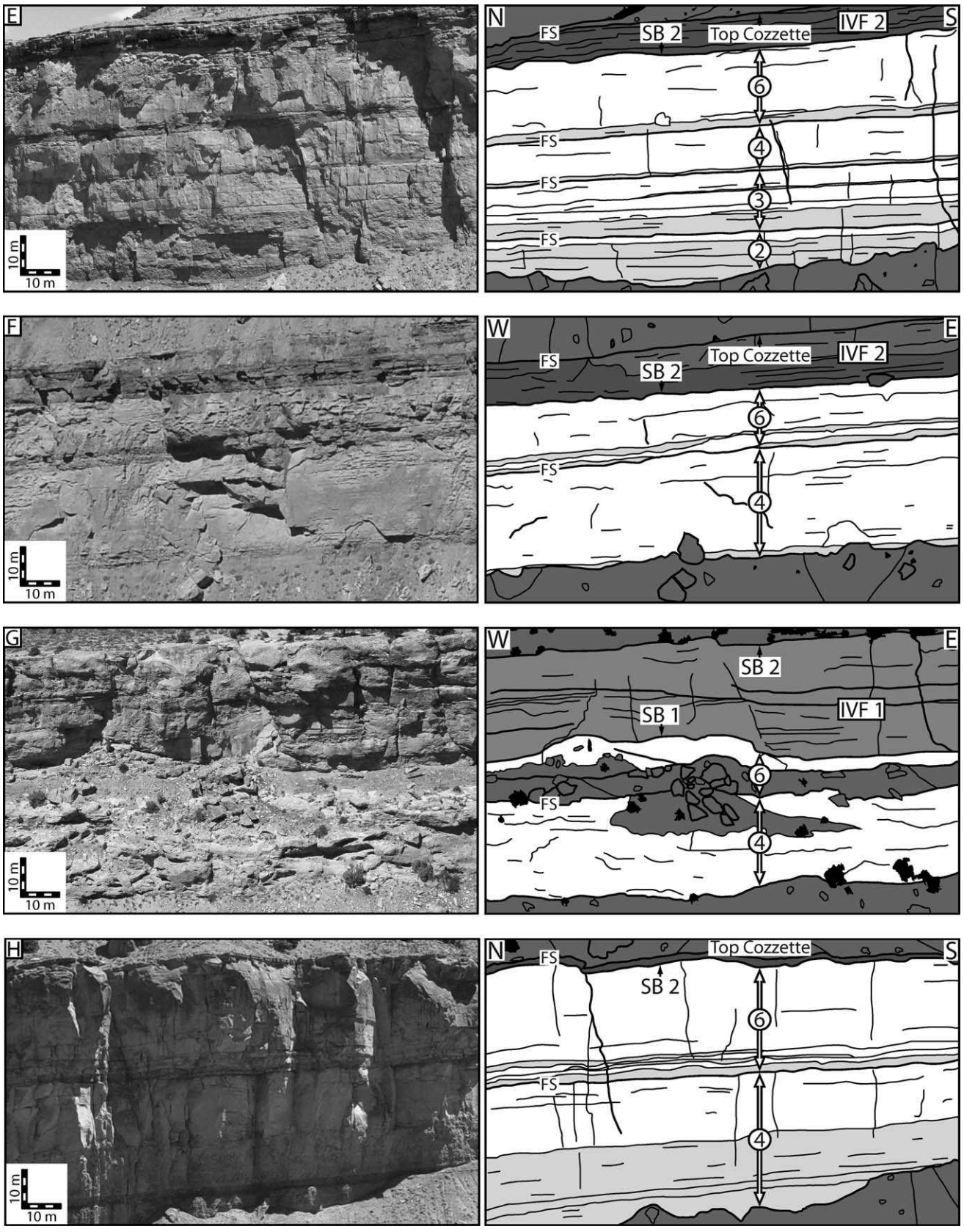

FIG 12.—Continued.

as the foundation for interpreting systems tracts. Parasequence stacking is assumed to be consistent in three dimensions, particularly in shallow marine settings. However, evidence from the Cozzette Sandstone suggests that changes in clinoform rollover position are spatially and temporally complex, and result in significant along-strike architectural changes.

Shallow marine deposits in the Cozzette Sandstone show a pronounced change in the trajectory of their rollover position and progradation direction with time (Figs. 16, 19). Capturing the inherent three dimensionality in the member consequently requires the use of multiple cross sections and isopach maps. Figure 19 illustrates the lateral change in parasequence stacking pattern from aggradational (west) to forestepping (east). Vertically stacked deposits (x–x′ in Fig. 19) show 20 km of rollover migration (from parasequence nos. 1 to 6), whereas shingled accumulations display 50 km of migration (z–z′ in Fig. 19).

A classical interpretation of Figure 19 would assign the aggradational deposits in the west to the transgressive and "early" highstand systems tract, and the time-equivalent forestepping accumulations in the east to the "late" highstand systems tract. Yet, this interpretation is inconsistent with the observation that the stacking pattern of systems tracts varies in three dimensions.

AGE

Age control in the Cozzette Sandstone consists of the late Campanian ammonites *Didymoceras nebrascense* and *Didymoceras stevensoni* (Gill and Hail 1975), as well as *Exiteloceras jenneyi* (Madden 1989). Gill and Hail (1975) collected *Didymoceras nebrascense* at Watson Creek, Colorado, either immediately below or at the base of the Cozzette, and *Didymoceras stevensoni* at Dirty George Creek and Stull Ditch, Colorado, towards the top of the member. Madden (1989) found *Exiteloceras jenneyi* at Rifle Gap, Colorado, at the base of the Rollins.

Ogg et al. (2004) established the North American western interior Late Cretaceous ammonite zones as follows: *Didymoceras nebrascense* (76.38–75.74 Ma); *Didymoceras stevensoni* (75.74–75.05 Ma); and *Exiteloceras jenneyi* (75.05–74.28 Ma). The fossil symbols in Figure 5 therefore indicate unknown points in time within the range of each ammonite zone. Owing to the paucity of specimens and the lack of diversity in the eastern Book Cliffs, specific information concerning the first and last occurrences of Cretaceous ammonites is unknown. Biostratigraphic ranges suggest an overall duration for the Cozzette (both depositional units and surfaces representing nondeposition and erosion) between 0.69 Myr and 2.1 Myr.

Late Campanian ammonites in the Cozzette Sandstone provide the following constraints (see Fig. 5). The presence of *Didymoceras nebrascense* (76.38–75.74 Ma) at the basal downlap surface and of *Didymoceras stevensoni* (75.74–75.05 Ma) at the top of parasequence no. 6 suggests that the six offlapping shallow marine deposits accumulated in less than 1.33 Myr, averaging ~ 220 kyr/cycle. That is comparable to the average span of a sequence in the underlying Sego Sandstone (150 kyr; Van Wagoner 1991b; see Fig. 4). Calculations of the average cycle length do not take into consideration unrepresented time in the stratigraphic record, or the nonlinearity of sediment accumulation (e.g., Miall 2014).

The occurrence of *Didymoceras stevensoni* (75.74–75.05 Ma) below sequence boundary no. 1 and of *Exiteloceras jenneyi* (75.05–74.28 Ma) above the uppermost Cozzette flooding surface implies that the fluvial and estuarine deposits represent an interval of 0–1.46 Myr. If two incised-valley fills are interpreted in the Cozzette Sandstone, each has an average duration of no more than 730 kyr.

COMPARISONS WITH PREVIOUS WORK

Previous outcrop and subsurface studies of the Cozzette Sandstone have yielded a wide variety of stratigraphic cross sections and depositional interpretations (Young 1955, 1966; Fisher et al. 1960; Warner 1964; Gill and Hail 1975; Collins 1976; Johnson 1979; Johnson et al. 1979a, 1979b, 1979c; Johnson 1986, 1989, 2003; Hettinger and Kirschbaum 2003; Patterson et al. 2003; Kirschbaum and Hettinger 2004; Madof 2006; Kamola et al. 2007; Cumella and Scheeval 2008; Aschoff and Steel 2011a, 2011b), but with similar paleoshoreline trends (Zapp and Cobban 1960; Warner 1964; Collins 1976; Johnson 1989, 2003; Franczyk 1989; Kennedy et al. 2000; Madof 2006). Existing interpretations suggest that sheet-like marginal marine to shallow marine strata consist of either one undifferentiated nearshore cycle (Young 1966; Gill and Hail 1975; Johnson 1986, 1989, 2003), or two (Young 1955; Warner 1964; Johnson et al. 1979a, 1979b; Cumella Scheevel 2008) or more (Kirschbaum and Hettinger 2004; Madof 2006; Kamola et al. 2007) cycles (see Fig. 20), up to 61 m (200 ft) thick (Warner 1964). Although the two- to three-cycle hypotheses are the most widely accepted, previous interpretations suggested that Cozzette paleoshorelines were close to straight, did not notably vary from one shoreface cycle to another, and trended either northeast (Zapp and Cobban 1960; Warner 1964; Collins 1976; Johnson 1989, 2003; Franczyk 1989; Kennedy et al. 2000) or north (Madof 2006; Kamola et al. 2007). Outcrop and subsurface data reported here indicate that rollover positions for offlapping deposits were straight to curvilinear (at kilometer scale) and exhibited a systematic change in trend from northeast to east (Fig. 16).

Differences in the interpretation of the stratigraphic architecture of the Cozzette Sandstone arise primarily through disparate approaches to correlation. Although previous workers did not explicitly state their methods, Madof (2006) drove into all accessible canyons between measured sections and used binoculars to trace surfaces on photographs. Figure 20, which is the product of this approach, has characteristics similar to a lithostratigraphic correlation and shows continuous tabular sandstone bodies. A comparison of Figure 20 with Figure 5 (constructed by tracing surfaces on high-resolution photographs and digital video) shows not only markedly dissimilar stratigraphic architecture but very different implied temporal relationships (Fig. 21). It is these spatial and temporal relationships that draw particular attention to the lateral extent and depositional processes responsible for the sheet-like shallow marine cycles (Fig. 22).

OFFLAP

Geometrical evidence from the Cozzette Sandstone suggests that offlapping shallow marine parasequences developed gradually via bypassing during sedimentation. This geometry, which is thought to develop via transport of sediment to the foreshore–shoreface in the absence of coastal-plain aggradation, has been created in numerical experiments (Prince and Burgess 2013) but is rarely seen in outcrop examples from siliciclastic systems. The Cozzette Sandstone therefore provides a unique look into this uncommon depositional phenomenon and its associated stratigraphic architecture (see Fig. 11 D–F).

Offlap surfaces in three dimensions lack laterally equivalent incised valleys and evidence for base-level lowering in the member. It is for this reason that offlap surfaces are not interpreted as the interfluve expression

→

FIG. 13.—Contour maps of compacted thicknesses (isopachs) of parasequences, created for the interval between downlap surface (mapped as flat) and overlying flooding surfaces no. 1 (A) through no. 5 (E). Note the positions and orientations of lines x–x′, y–y′, and z–z′, which were used to create Figures 15, 18, and 19. Dotted lines represent positions of rollover. Parasequences nos. 2, 4, and 5 show back-tilting from rollover to offlap (Fig. 13B, D, E). Structure of the Piceance basin was subtracted for each map. Contour interval is 5 ft (1.5 m).

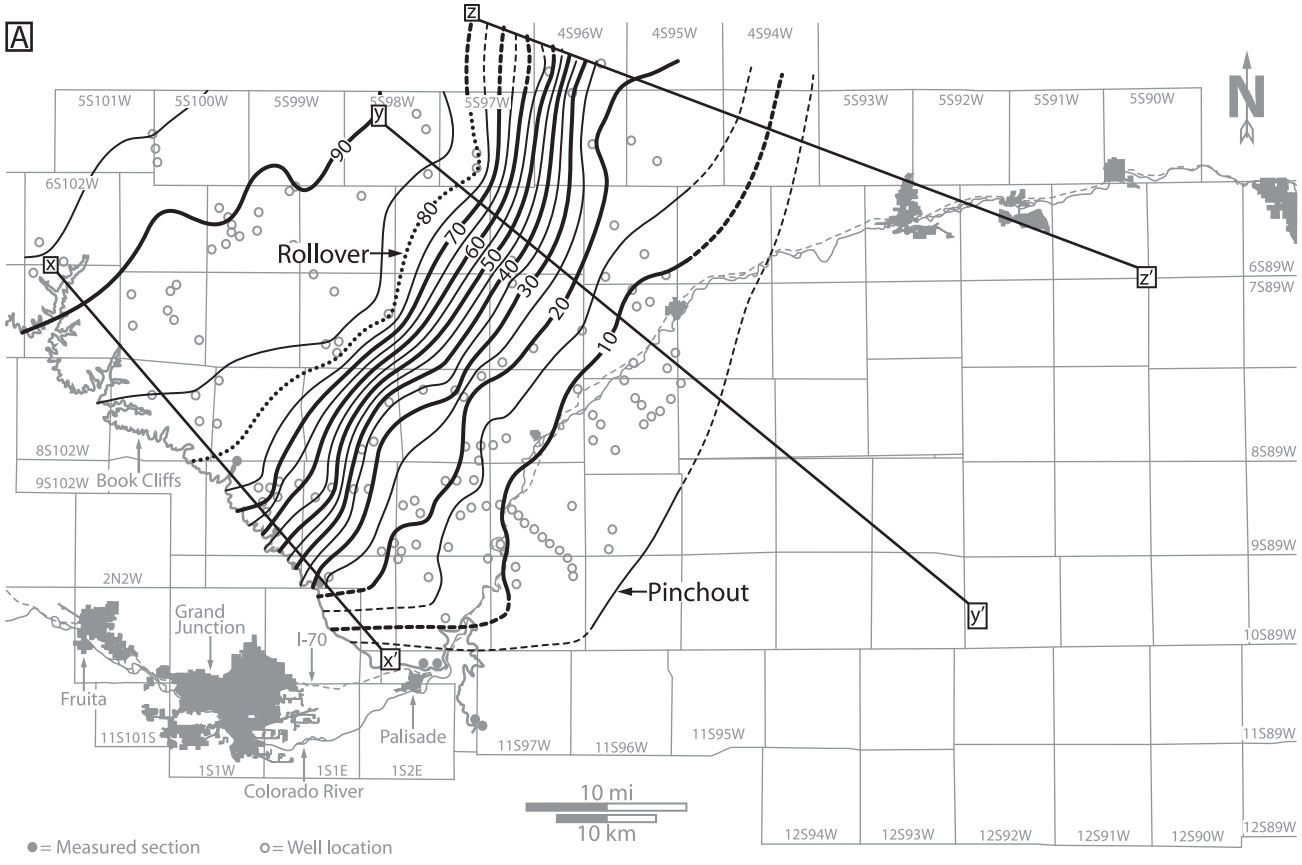
A
z
y
x
z'
y'
x'
90
80
70
60
50
40
30
20
10
Rollover
Pinchout
N
4S96W
4S95W
4S94W
5S101W
5S100W
5S99W
5S98W
5S97W
5S93W
5S92W
5S91W
5S90W
6S102W
6S89W
7S89W
8S102W
9S102W
Book Cliffs
8S89W
9S89W
2N2W
Grand Junction
I-70
Fruita
11S101S
Palisade
1S1W
1S1E
1S2E
Colorado River
11S97W
11S96W
11S95W
11S89W
10S89W
12S94W
12S93W
12S92W
12S91W
12S90W
12S89W
10 mi
10 km
● = Measured section
○ = Well location

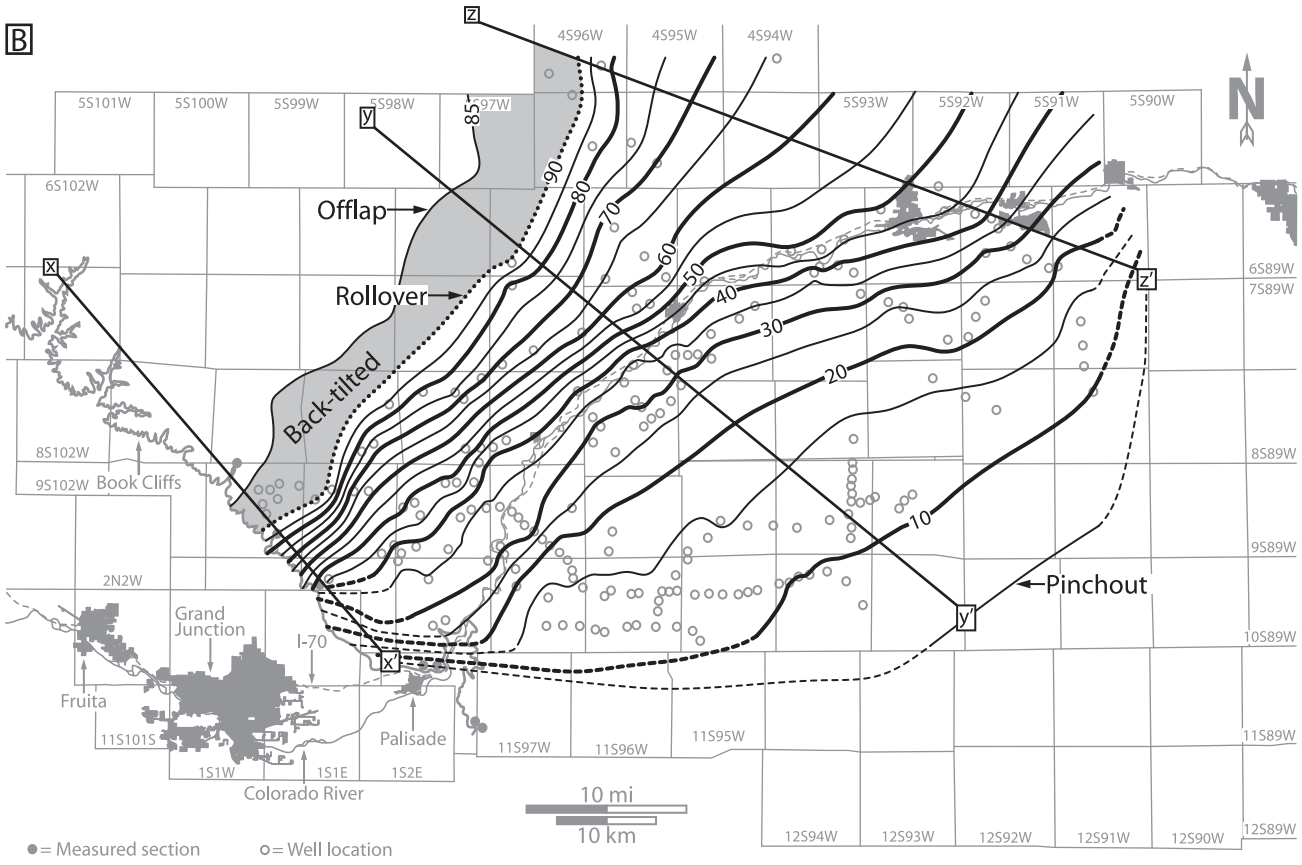
B
z
y
x
z'
y'
x'
85
90
80
70
60
50
40
30
20
10
Offlap
Rollover
Back-tilted
Pinchout
N
4S96W
4S95W
4S94W
5S101W
5S100W
5S99W
5S98W
5S97W
5S93W
5S92W
5S91W
5S90W
6S102W
6S89W
7S89W
8S102W
9S102W
Book Cliffs
8S89W
9S89W
2N2W
Grand Junction
I-70
Fruita
11S101S
Palisade
1S1W
1S1E
1S2E
Colorado River
11S97W
11S96W
11S95W
11S89W
10S89W
12S94W
12S93W
12S92W
12S91W
12S90W
12S89W
10 mi
10 km
● = Measured section
○ = Well location

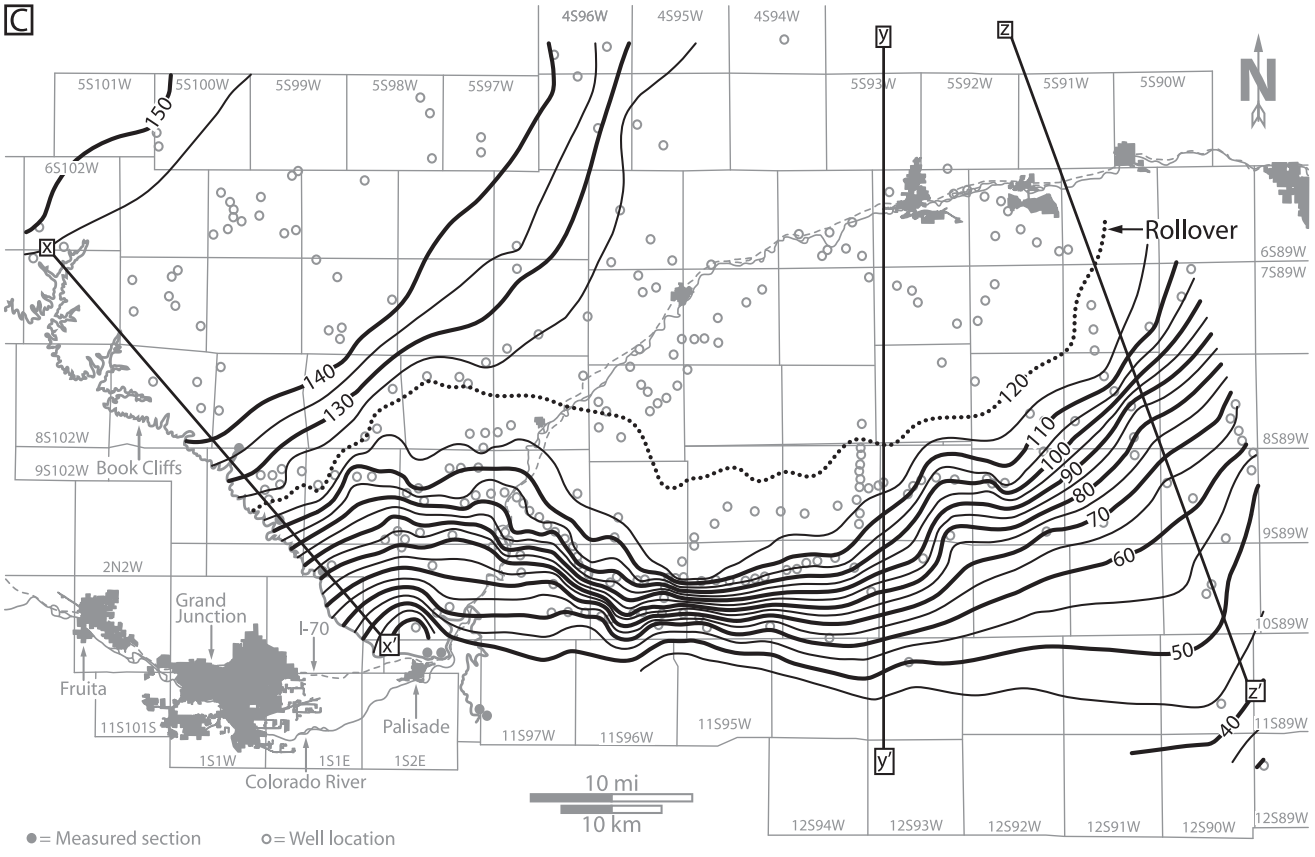

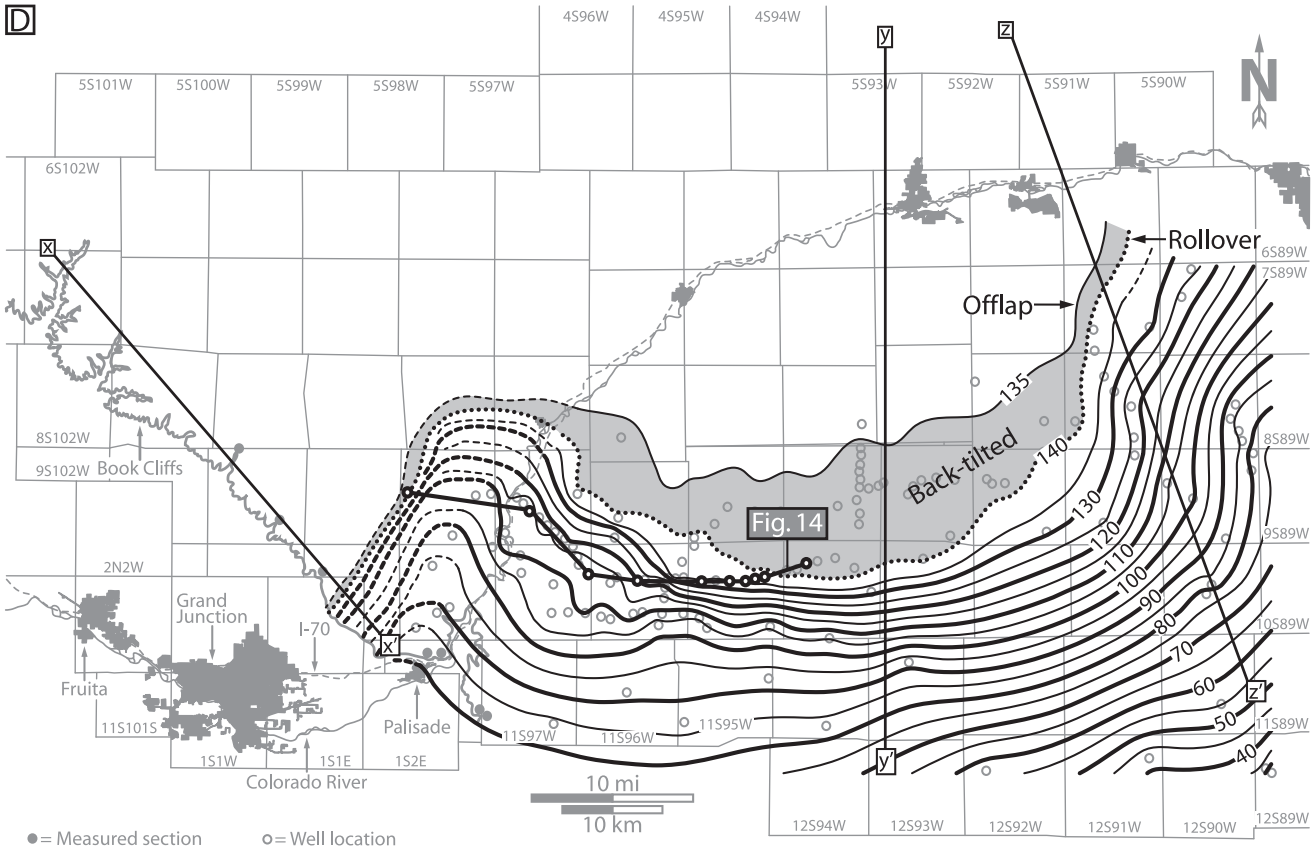

FIG 13.—Continued.

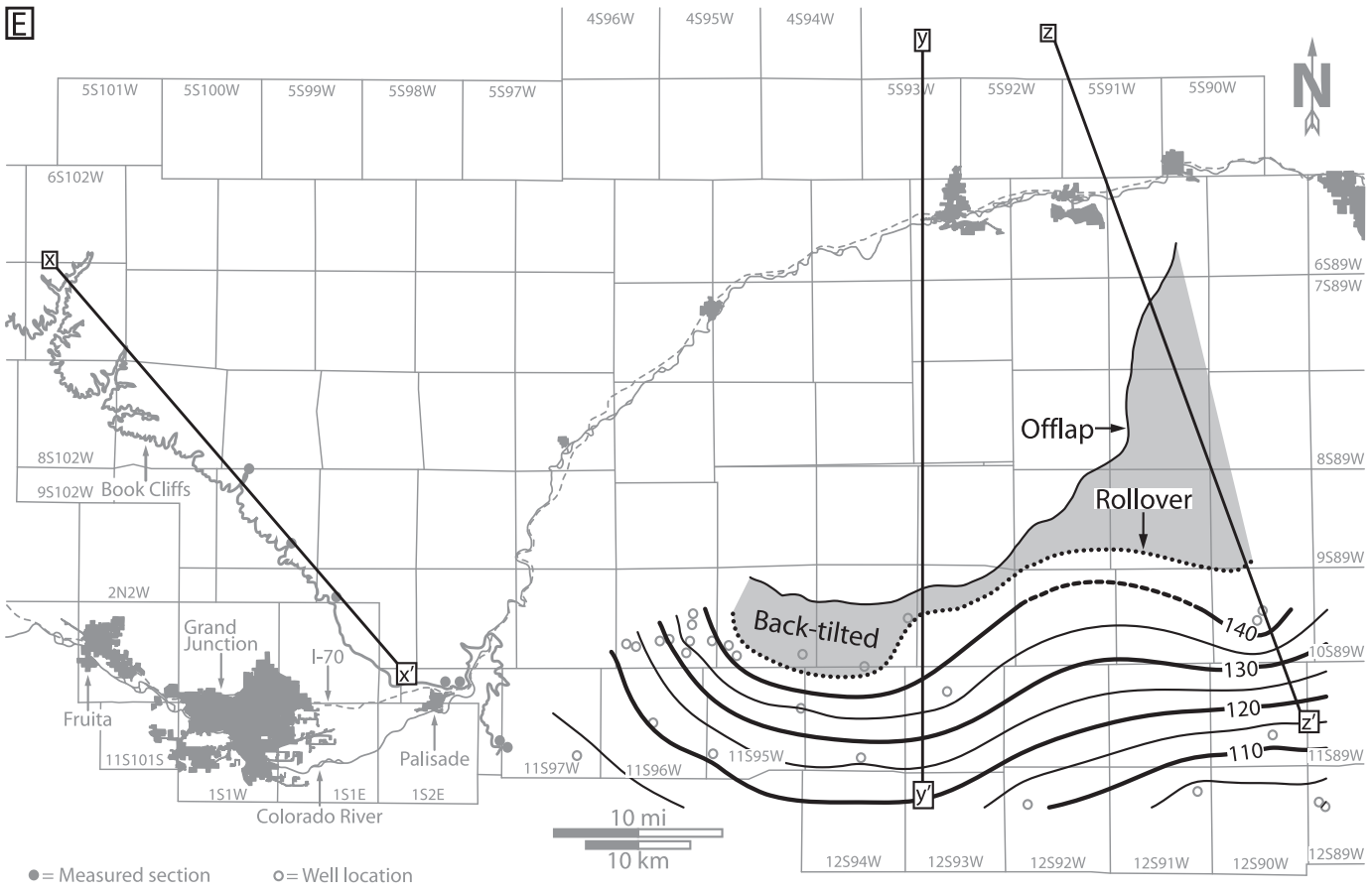

FIG 13.—Continued.

of sequence boundaries, but as parasequence and parasequence set boundaries.

STRATIGRAPHIC CONTROLS

Syndepositional to postdepositional tectonic tilting in the southern Piceance basin better explains changes in depositional orientation, shifts in rollover trends, and the formation of sequence boundaries than currently accepted sequence stratigraphic models concerned with the interaction between varying rates of sea-level change and regional patterns of flexural subsidence. This mechanism also accounts better for the three-dimensional arrangement and distribution of shallow marine parasequences and incised-valley fills. The development of the Cozzette Sandstone should therefore be regarded in terms of variation in the directions of tilt and progradation in an actively deforming basin (Fig. 23).

Eustasy and Subsidence

Sequence stratigraphic models applied to foreland basins suggest that nearshore accommodation is controlled by the interaction between varying rates of eustatic change and regional patterns of flexural subsidence caused by thrust-sheet loading (Posamentier and Allen 1993; Willis 2000; Castle 2001; Hoy and Ridgway 2003; Atchley et al. 2004; Escalona and Mann 2006; Bera et al. 2008). In this view, short- and long-term patterns of subsidence are assumed to be identical, such that in areas proximal to the thrust load, subsidence consistently exceeds the pace of eustatic fall, whereas in areas distal to the orogenic belt, the rate of sea-level fall is greater than the rate of subsidence at least part of the time. These interactions are thought ultimately to control the distribution of systems tracts, which are defined and identified on the basis of position within a sequence, parasequence stacking patterns, and types of bounding surfaces (see Van Wagoner et al. 1990; Van Wagoner 1995).

In order to test sequence stratigraphic models, both Cretaceous sea-level change and Sevier thrusting must be evaluated. Backstripped eustatic estimates from New Jersey and the Russian platform document large (i.e., more than 25 m/82 ft) and rapid (i.e., less than ~ 1 Myr) eustatic oscillation during greenhouse conditions (Miller et al. 2004; Miller et al. 2005b; Fig. 24) and are interpreted to record volume changes of Late Cretaceous Antarctic ice sheets. Comparisons of $\delta^{18}O$ values from benthic foraminifera with modeling results suggest that a Late Cretaceous ice sheet no greater than 25–50% of the size of the current east Antarctic ice sheet was restricted to the interior of the continent and existed only during short intervals of peak Milankovitch insolation (i.e., 100 kyr duration). Antarctica may have been relatively ice-free during much of the greenhouse conditions of the Late Cretaceous.

During this time in central Utah, regional shortening was accommodated on the eastward-propagating (i.e., in-sequence) frontal Paxton and Gunnison thrust systems (DeCelles et al. 1995; DeCelles and Coogan 2006). Both thrusts, identified in seismic and well-log data, are blind west-dipping faults that fed slip into a frontal triangle zone. The Paxton thrust sheet was emplaced during the Santonian, and the Paxton duplex was formed during the early to middle Campanian, and possibly through the late Campanian. The Paxton thrust is thought to have produced a major topographic plateau, which supplied sediment to the Cretaceous interior foreland basin through the Paleocene. The Gunnison thrust system is interpreted to have been active from the late Campanian to the early Paleocene.

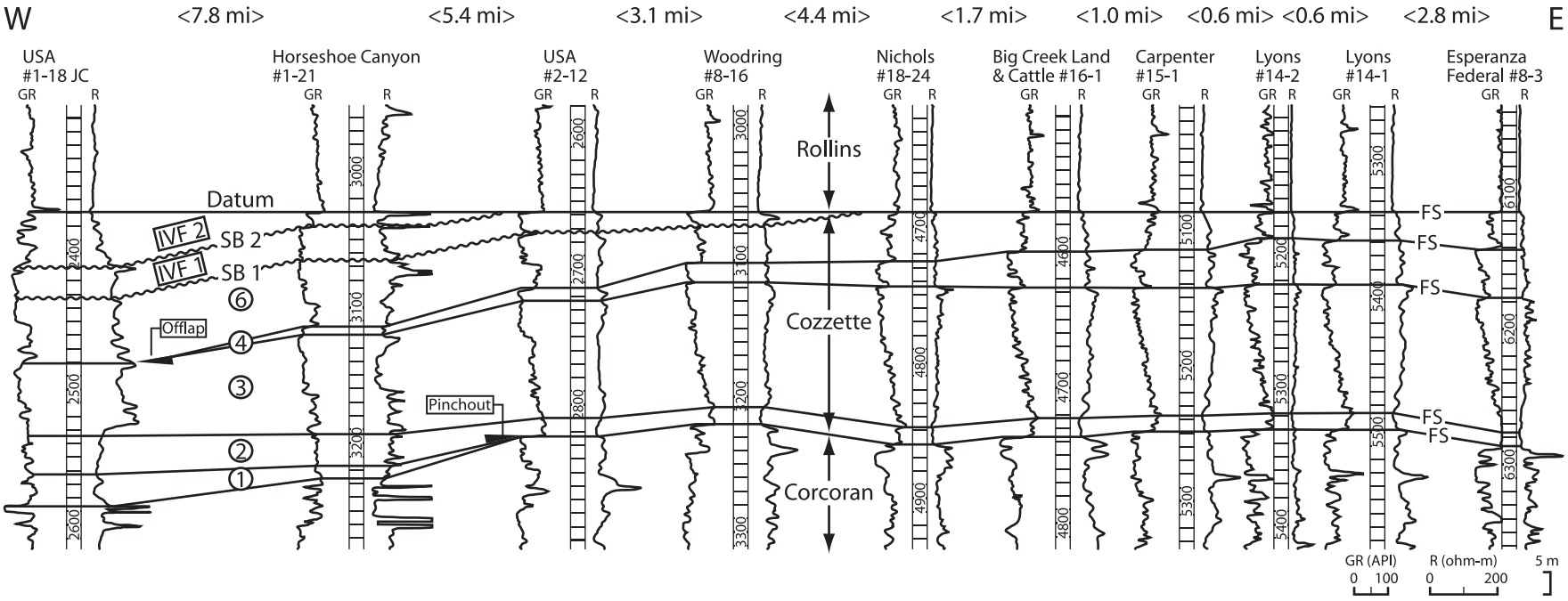

FIG. 14.—East–west oriented well-log cross section, showing log signature of the Cozzette Sandstone in the south-central study area. (See Figs. 2 and 13D for map location of cross section.) Parasequence no. 4 offlaps between the USA #1-18 JC and Horseshoe Canyon #1-21 wells, whereas no. 1 displays pinchout by downlap between the Horseshoe Canyon #1-21 and USA #2-12 wells. Compare the subsurface geometry of this figure to the outcrop expression of offlap and pinchout (offlap, Fig. 11A–D; downlap, Fig. 11E–F). Abbreviations are the same as used in Figure 5. GR, Gamma ray; R, Resistivity; API, American Petroleum Institute units.

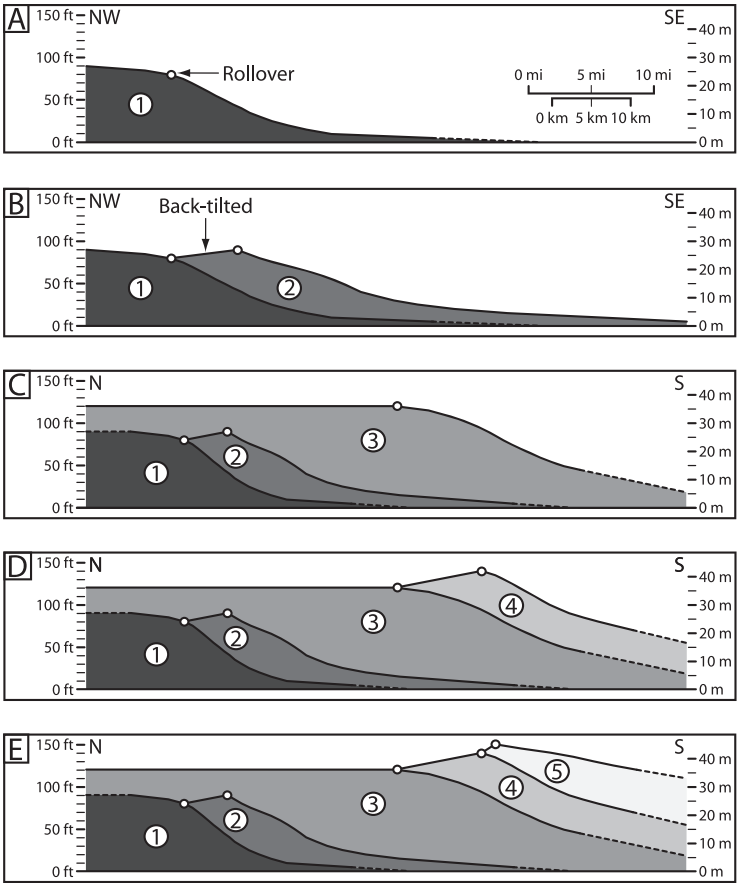

FIG. 15.—Cross sections showing development of parasequence no. 1 (A) through no. 5 (E), created from line y–y′ in Figure 13. Rollover positions are geometrically defined by a break in slope. Note the back-tilted orientation (landward of the rollover) of parasequence boundaries nos. 2, 4, and 5, which is observed in map view in Figures 13B, D, and E. Back-tilted geometry relates to the structural stratigraphic evolution of the Cozzette Sandstone (discussed in Stratigraphic Controls section).

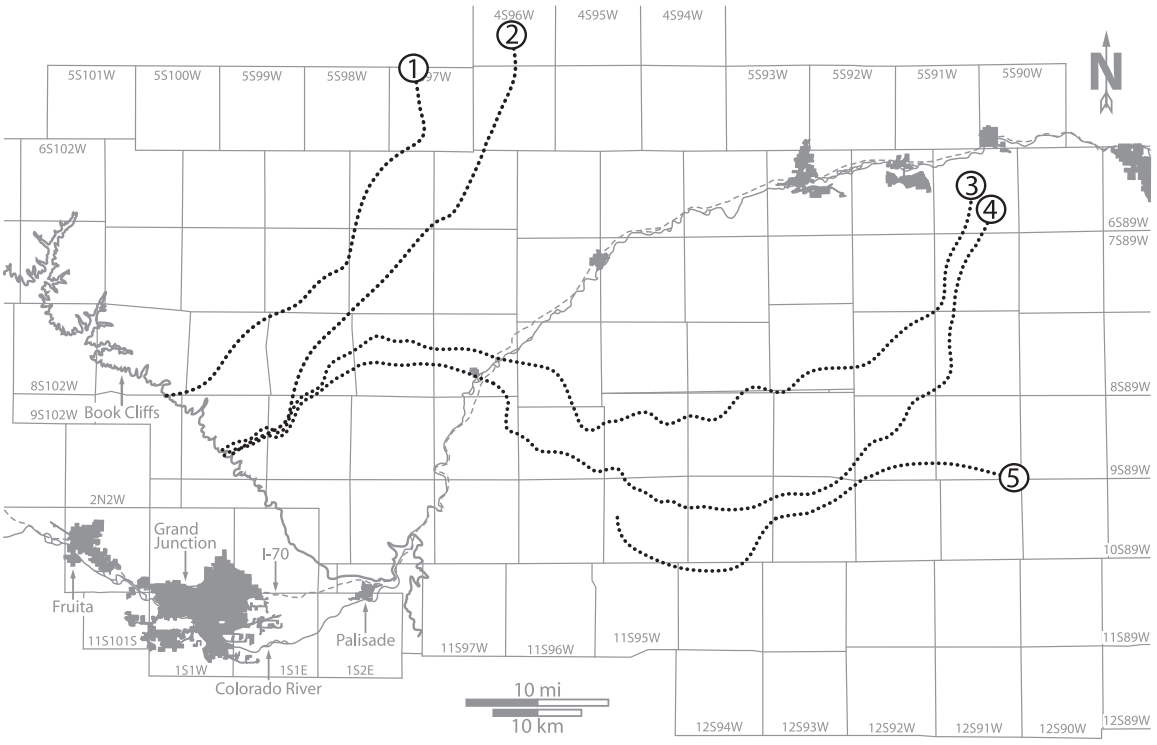

FIG. 16.—Rollover positions through time for parasequences nos. 1 through 5, taken from Figure 13, showing a linear northeast trend for parasequences nos. 1 and 2 and an irregular east orientation for parasequences nos. 3, 4, and 5. Note that rollover positions progressively step basinward (southeast) through time.

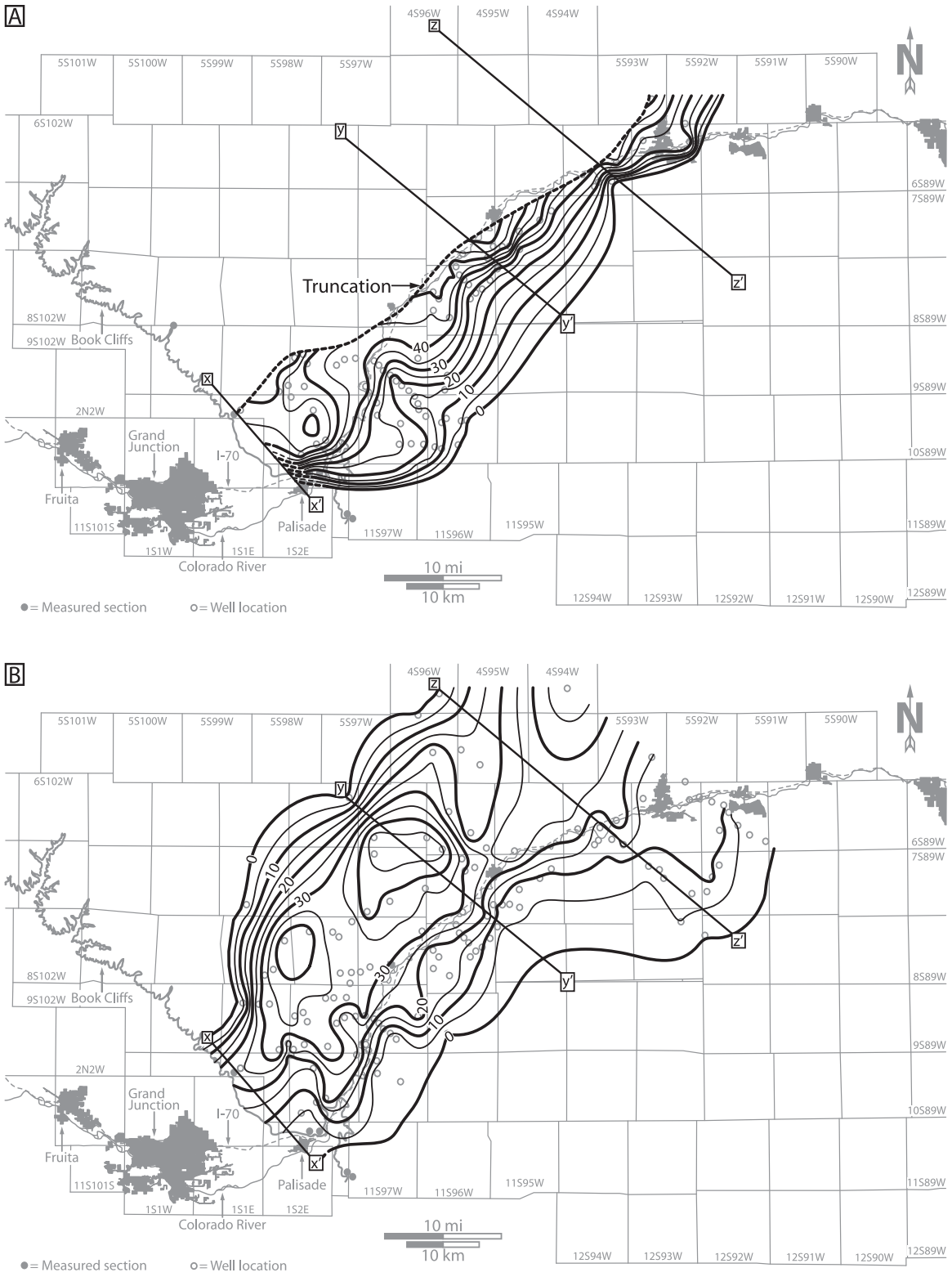

FIG. 17.—Contour maps of compacted thicknesses (isopachs) of incised valley(s), created for the interval between the last Cozzette flooding surface (mapped as flat) and underlying erosional surfaces. Note the positions and orientations of lines x–x′, y–y′, and z–z′, which were used to create Figures 18, and 19. Structure of the Piceance basin was subtracted for each map. Contour interval is 5 ft (1.5 m). **A)** Isopach map of truncated incised valley no. 1, mapped between top Cozzette flooding surface and underlying sequence boundary no. 1. Note truncation (dashed line) by overlying sequence boundary (or scour). Where the fluvial valley fill is preserved, it reaches a maximum thickness of 63.9 ft (19.5 m) and thins to the southeast. **B)** Isopach map, created between top Cozzette flooding surface and underlying sequence boundary no. 2 (or scour). The estuarine deposits have a northeast-oriented axis and reach a maximum thickness of approximately 47.9 ft (14.6 m).

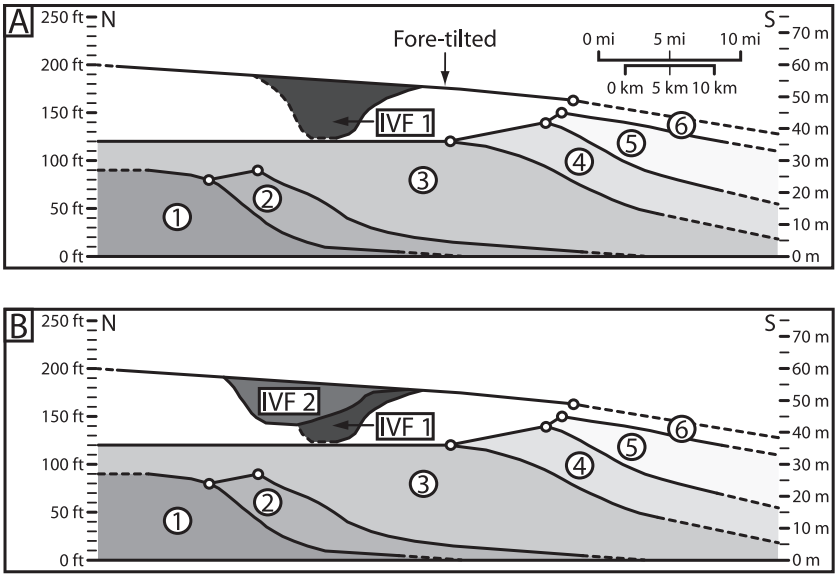

FIG. 18.—Cross sections showing development of incised valleys **A)** no. 1 and **B)** 2, created from line y–y′ in Figure 13. Fore-tilted geometry relate to the depositional and deformational evolution of the Cozzette Sandstone (see Stratigraphic Controls section).

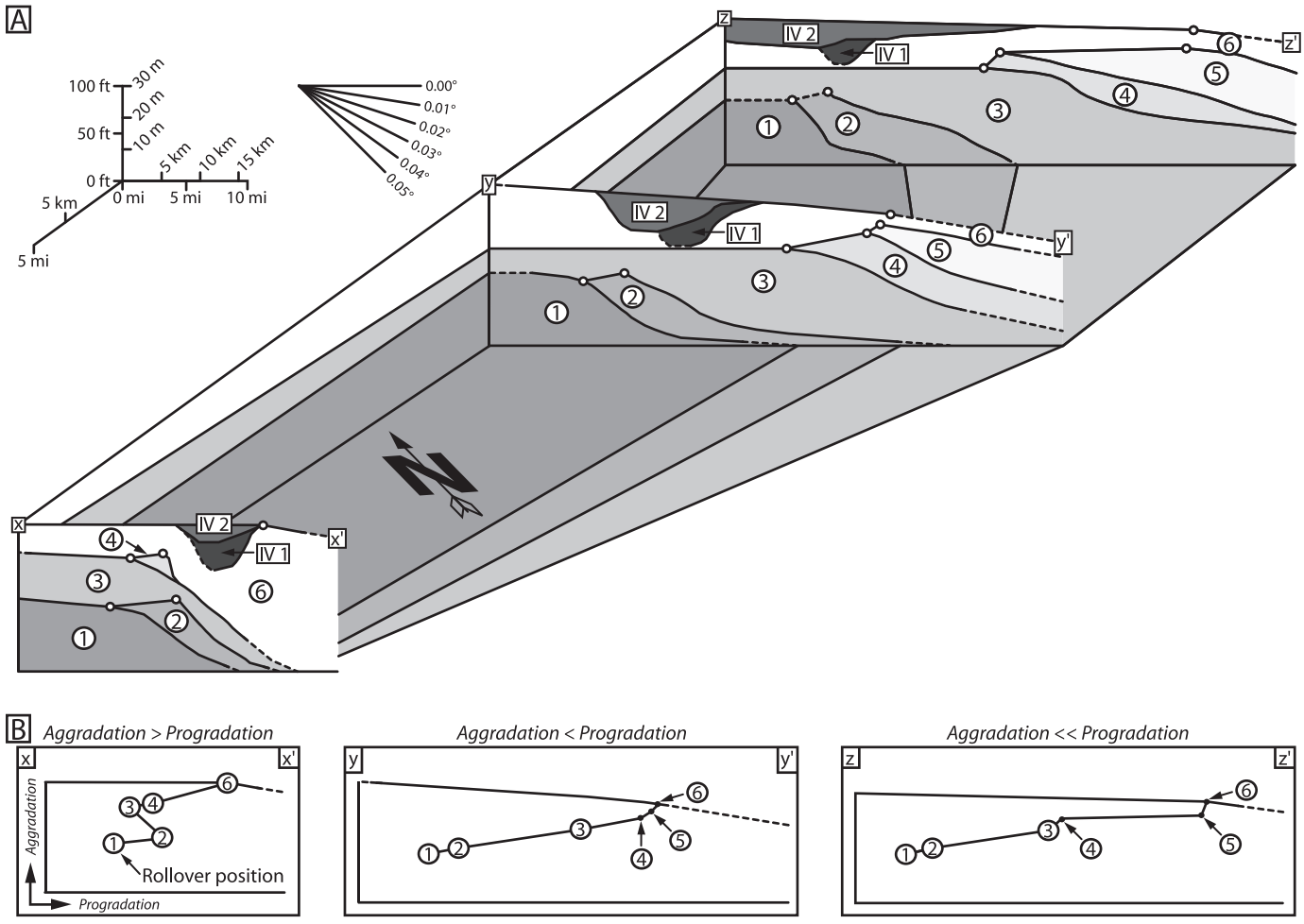

FIG. 19.—Fence diagram showing **A)** 3D stratigraphy and **B)** 2D rollover trajectory of the Cozzette Sandstone. Illustration was drawn from lines x–x′, y–y′, and z–z′ in Figure 13. **A)** Oblique view, looking northeast, showing stratigraphic architecture of the member. Parasequences extend farther basinward in the eastern part of the southern Piceance basin. **B)** Cross sections showing west–east change in rollover trajectory and parasequence stacking patterns. In the west, parasequences display aggradation (x–x′), whereas in the east they show marked progradation (y–y′ and z–z′).

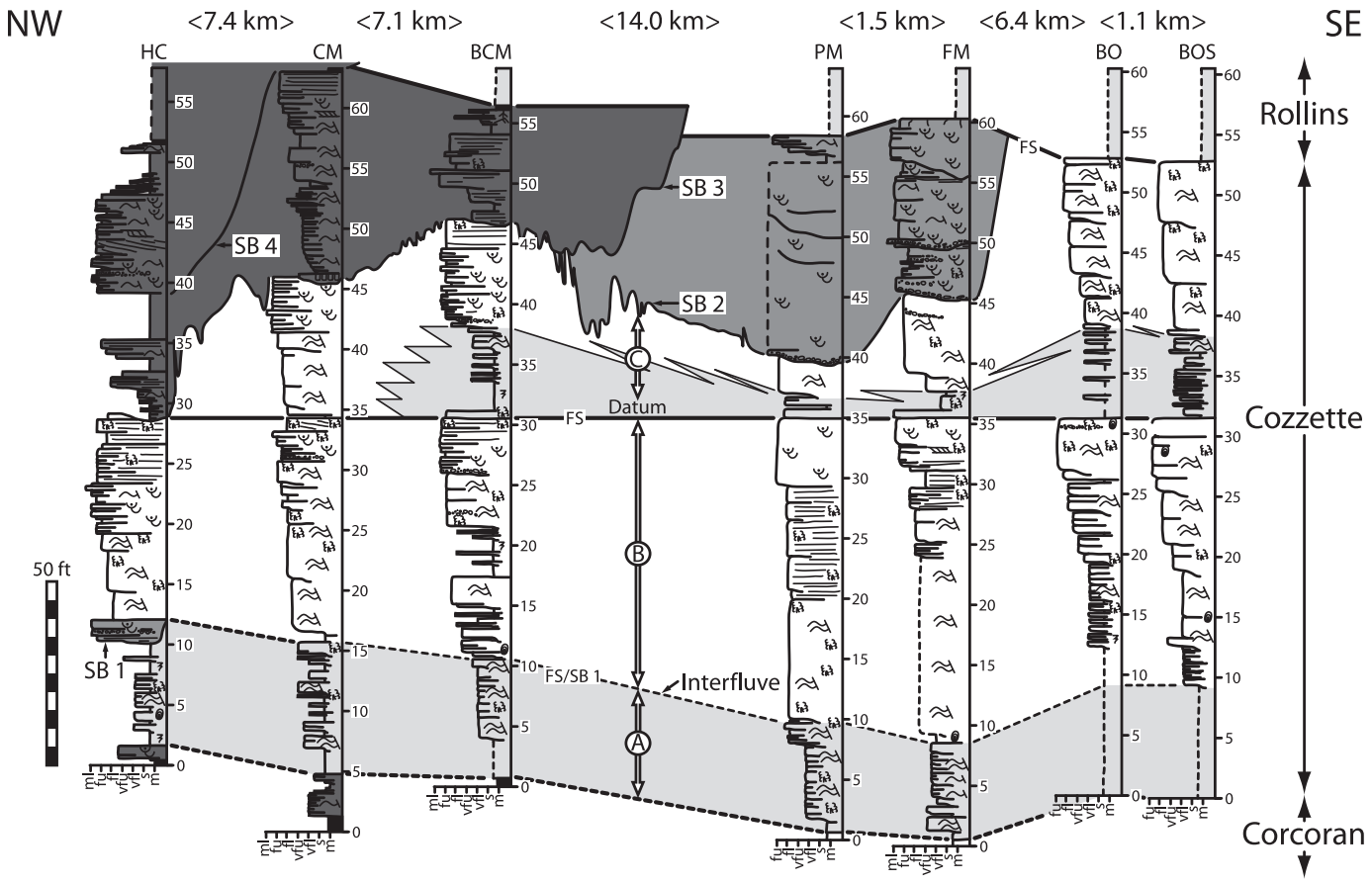

FIG. 20.—An earlier sequence stratigraphic interpretation of the Cozzette Sandstone (redrawn from Madof 2006). Measured sections were correlated between canyons, kilometers away from Cozzette outcrops, by tracing surfaces with binoculars. See Figure 2 for measured section abbreviations and Figure 5 for abbreviations and color scheme of interpreted depositional environments. Circled letters A–C denote shallow marine parasequences; SB1–SB4 refers to sequence boundaries (erosional); and FS indicates flooding surfaces.

Comparing timing of Cretaceous sea-level change and Sevier thrusting demonstrates that sequence stratigraphic models are not only difficult to employ but also fail in the context of the Cozzette Sandstone. Specifically, it is unclear from these conceptual models if thrust-sheet emplacement causes initial proximal erosion followed by sediment and tectonic loading, or initial tectonic subsidence followed by proximal erosion (cf. Heller et al. 1988). Timing of emplacement of a tectonic load therefore leads to either immediate or delayed subsidence patterns. Yet neither view, when compared to sea-level change, can adequately account for the stratigraphic architecture of the Cozzette Sandstone.

TABLE 4.—*Three basinward-landward tilting cycles in the Cozzette Sandstone.*

Subsidence Direction	Cycle No. 1
Basinward - southeast	Parasequence No. 1
Landward - north	Parasequence No. 2
Basinward - south	Parasequence No. 3
Subsidence Direction	**Cycle No. 2**
Basinward - south	Parasequence No. 3
Basinward - south	Parasequence No. 4
Landward - north	Parasequence No. 5
Basinward - southwest	Parasequence No. 6
Subsidence Direction	**Cycle No. 3**
Basinward - southwest	Parasequence No. 6
Basinward - southwest	Incised valley fill No. 1
Landward - northeast	Incised valley fill No. 2

Available estimates of late Campanian sea-level change (Fig. 24) suggest that shallow marine parasequences accumulated during times of both falling and rising sea level (i.e., 76.38–75.74 Ma), whereas fluvial and estuarine deposits accumulated during times of rising and falling sea level (i.e., 75.74–74.28 Ma). In order for the observed stratal patterns to develop, existing sequence stratigraphic models would require subsidence (i.e., a relative high stand of sea level) during 76.38–75.74 Ma, followed by uplift (i.e., a relative low stand of sea level) from 75.74 to 74.28 Ma. Based on its position in the foredeep and distance from the flexural bulge (cf. DeCelles and Coogan 2006), it is unreasonable to assume that western Colorado underwent the needed flexurally induced uplift at 75.74 Ma. Accordingly, prior to this time, thrusting-induced subsidence from the Paxton duplex would not have had any major effect on Cozzette deposition, as the structure had limited areal extent and was restricted to west-central Utah (Fig. 24).

Tilting

Tilting during and after deposition of the Cozzette Sandstone can be determined from parasequence architecture and stratigraphic geometry more generally. For example, tilting during deposition would create differentially overthickened parasequences, resulting in

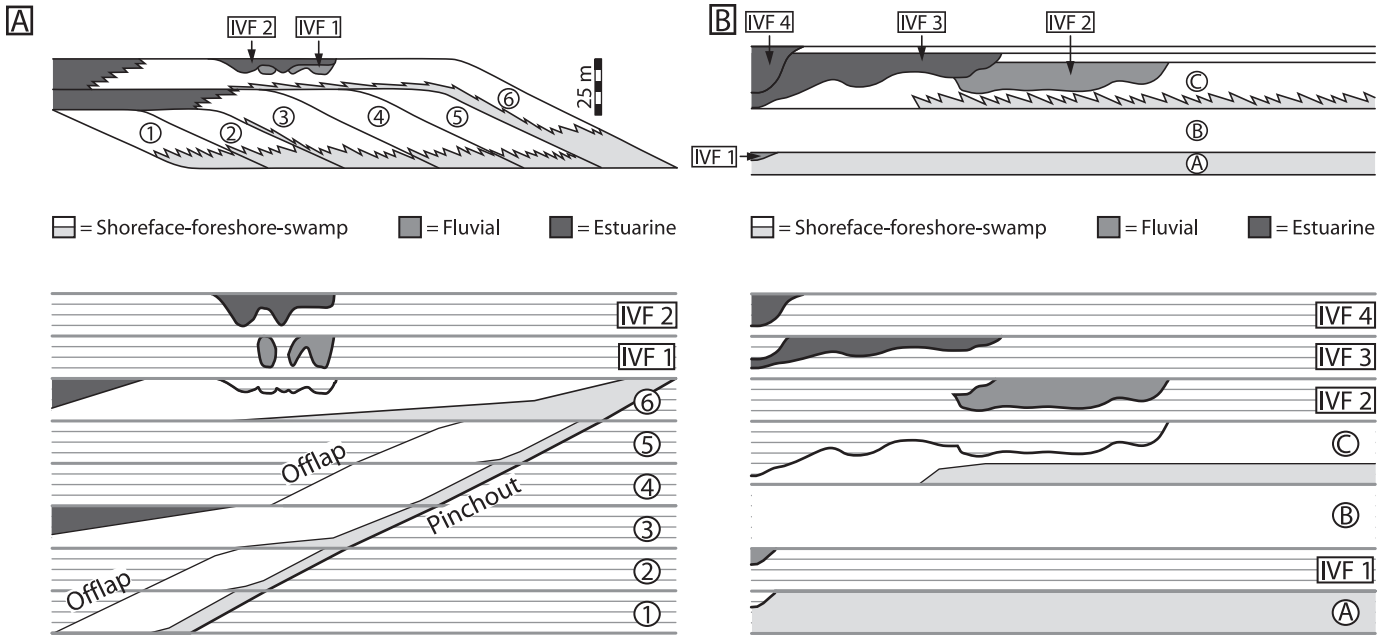

FIG. 21.—Simplified sequence stratigraphic architecture and associated Wheeler diagram for proposed (Fig. 5) and previous (Fig. 20) interpretations of the Cozzette Sandstone. Circled numbers and letters denote shallow marine parasequences and IVF1–IVF4 signify incised-valley fills. See Figure 5 for color scheme of interpreted depositional environments. **A)** Proposed interpretation recognizes six offlapping parasequences of approximately equal duration, overlain by incised-valley fill located at the top of the member. Based on available age control, formation of the sequence boundary and incised-valley fill took longer than the six underlying deposits. Note that bypass leads to nondeposition landward of offlap, whereas lack of terrigenous input produces hiatuses basinward of pinchout by downlap. **B)** The earlier interpretation identifies three sheet-like and tabular parasequences of unequal duration, overlain by four incised-valley fills (three of which are located at the top of the member). Note the presence of IVF1 above parasequence A.

growth geometry parallel to the subsidence direction. In contrast, postdepositional tilting would lead to asymmetric accommodation, resulting in compensatory and shingled shallow marine deposits. Because this level of detail (overthickening vs. compensation) is difficult to discern given the scale of observation, we recognize both syndepositional and postdepositional tilting as possible controlling mechanisms on deposition.

Three cycles of basinward-landward tilting in the southern Piceance basin (Table 4) are interpreted to have led to systematic changes in sediment transport directions responsible for controlling accumulation of the Cozzette Sandstone (Fig. 25). During the deposition of parasequence no. 1, progradation to the southeast was associated with a northeast trending rollover orientation (Fig. 25A). The arrows in Figure 25A show the subsidence vectors needed to create the block diagram in Figure 25B, and highlight syndepositional to postdepositional tilting in a basinward direction. The arrows in Figure 25B show a landward reversal in tilting, which is interpreted to have resulted in new accommodation up-dip, space that was eventually filled by deposits of the next cycle (Fig. 25C).

Renewed basinward tilting began during or after the deposition of parasequence nos. 3 and 4 (Fig. 25D). It continued through to the accumulation of no. 5 (Fig. 25E). A change towards landward tilting (arrows in Fig. 25E) again created new accommodation towards the north, resulting in the development of parasequence no. 6 (Fig. 25F). This interval marks the beginning of the third cycle.

Although gradients calculated from thickness maps (see Stratigraphic Architecture section) do not represent true depositional dip of flooding surfaces, as compaction leads to underestimations of inclination, parasequences no. 2 and no. 4 yield landward tilts of 0.02° and 0.08°, respectively. These inclinations were measured in two dimensions (from offlap to rollover) from Figure 5. Assuming that the average duration of a Cozzette shoreface–foreshore–swamp parasequence (and associated hiatuses) is less than 221 kyr (see Age section), landward tilting rates are between 0.4°/Myr and 0.1°/ Myr. Considerably higher rates of tilting are calculated from outcrops from the Maghrebian thrust belt, central Sicily, in which offlapping late Pliocene shallow marine carbonate cycles progressively tilted at an average rate of 36°/Myr (Lickorish and Butler 1996). Lickorish and Butler (1996) concluded that tilting was controlled by active uplift of the southern limb of the Marcasita anticline.

Changes in the rate and location of tilting in the southern Piceance Basin are interpreted to have been responsible for the development of tectonically induced sequence boundaries in the Cozzette Sandstone (Fig. 25G–H). Relatively large magnitudes of tilting in a basinward

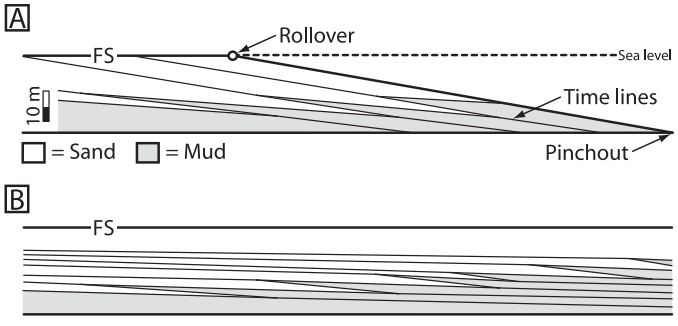

FIG. 22.—Cross section of idealized shallow marine parasequence from proposed (Fig. 5) and previous (Fig. 20) interpretations of the Cozzette Sandstone. FS indicates a flooding surface. **A)** Proposed interpretation recognizes wedge-shaped geometry of nearshore parasequences. **B)** Previous interpretation envisions accumulation as sheet-like.

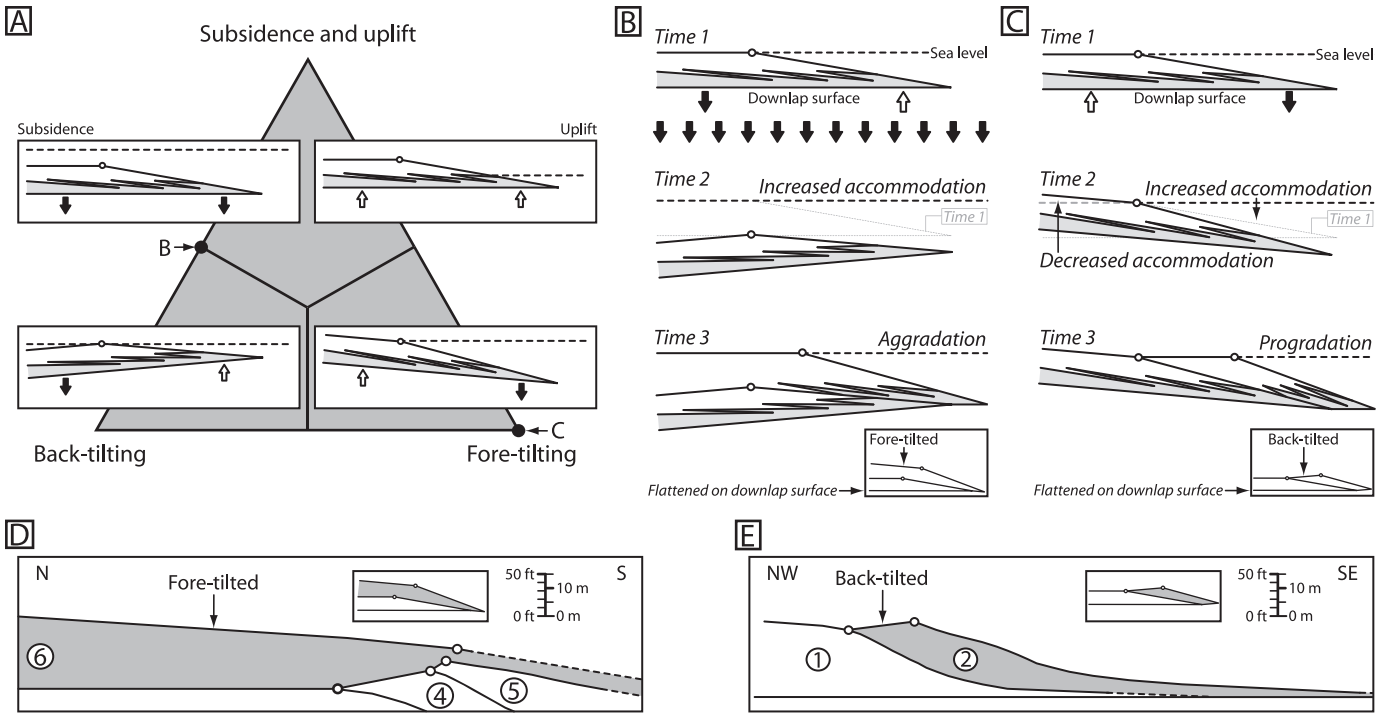

FIG. 23.—Structural stratigraphic model showing the influence of tilting on deposition. Note that stratigraphic geometry in the Cozzette Sandstone includes both depositional and deformational components. **A)** Ternary diagram illustrating the effect of both uniform and differential subsidence on stratigraphic architecture. Note the positions of B and C. **B)** Depositional model showing development of shallow marine parasequence (Time 1), followed by subsidence, back-tilting (Time 2), and deposition of a second parasequence (Time 3). Note that flattening on downlap surface tilts the depositional geometry basinward (fore-tilt, see inset). **C)** Depositional model highlighting the effect of fore-tilting on differential accumulation. Subsequent to parasequence deposition (Time 1), fore-tilting creates increased accommodation basinward of the rollover, and the opposite effect landward of that point (Time 2). The next parasequence (Time 3) is subsequently deposited atop the underlying and tilted deposit. Hence, flattening on the downlap surface (see inset) gives the appearance of back-tilting landward of the rollover. **D**, **E)** Comparison of depositional models in Parts B and C (inset) to geometry of parasequence no. 6 (Fig. 18A) and no. 2 (Fig. 15B), respectively.

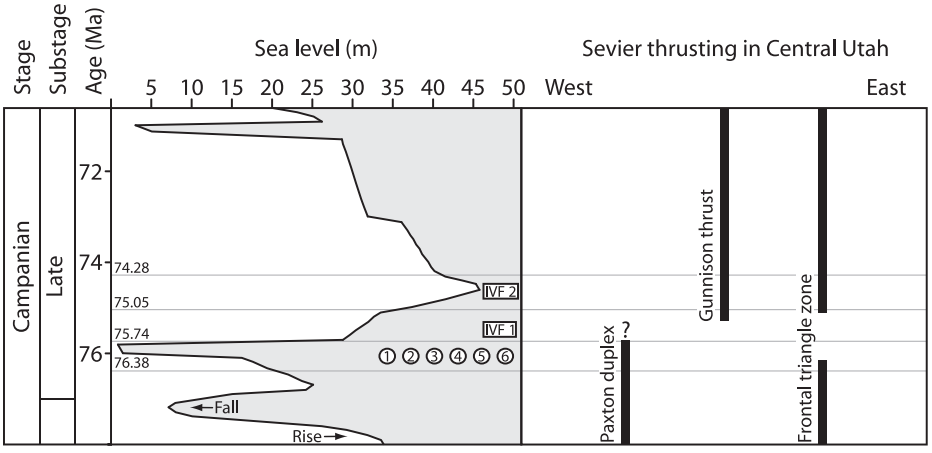

FIG. 24.—Sea-level curve (eustasy plus water loading) (Miller et al. 2005a) and Sevier thrusting episodes in central Utah (DeCelles and Coogan 2006) during middle to late Campanian. Timescale is from Ogg et al. (2004). Ages are as follows: 76.38–75.74 Ma (*Didymoceras nebrascense*) at the base of the Cozzette, or immediately below; 75.74–75.05 Ma (*Didymoceras stevensoni*) at the top of parasequence no. 6; and 75.05–74.28 Ma (*Exiteloceras jenneyi*) at the base of the Rollins (i.e., above top Cozzette flooding surface). See Figure 5 for distribution of age control. Note that shoreface–foreshore–swamp parasequences develop during falling, low stand, and rising sea level, whereas fluvial and estuarine accumulations form during rising, high stand, and falling sea level.

→

FIG. 25.—Stratigraphic evolution of the Cozzette Sandstone. Conceptual three-dimensional block diagrams showing the effect of three cycles of basinward-landward tilting (see Table 4) on sediment accumulation. Tilting to the south causes the direction of progradation to change from **A**, **B)** southeast to **C**–**F)** south, and the orientation of rollovers to shift from **A**, **B)** northeast to **C**–**F)** east. A change in tilting towards the north creates landward accommodation and deposition of overlying parasequences (C and F). Subsidence to the southwest generates tectonically induced sequence boundaries, fluvial (G) and estuarine deposition (H), and transport in that direction.

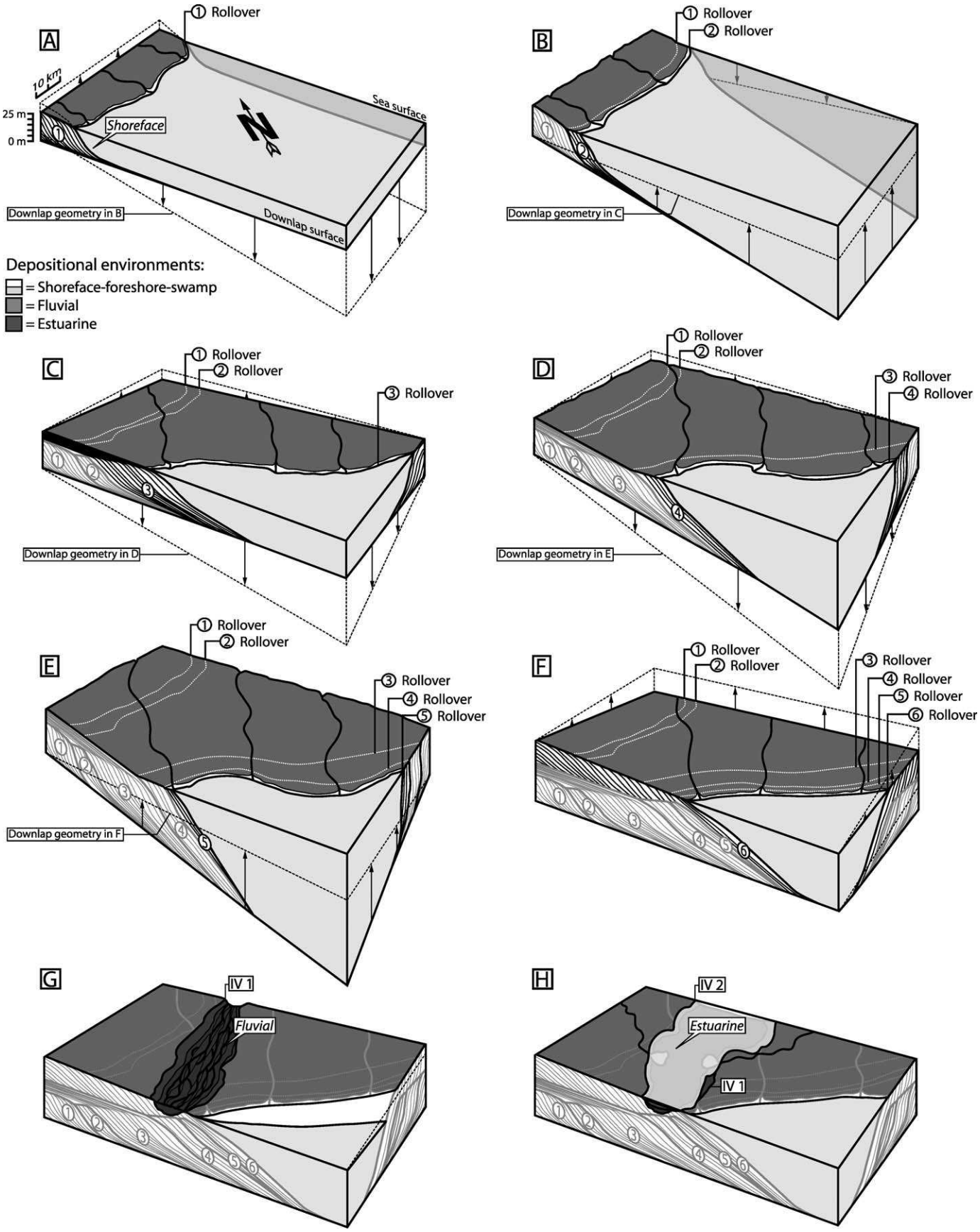
A
① Rollover
10 km
25 m
0 m
Shoreface
Sea surface
Downlap geometry in B
Downlap surface
Depositional environments:
= Shoreface-foreshore-swamp
= Fluvial
= Estuarine
B
① Rollover
② Rollover
Downlap geometry in C
C
① Rollover
② Rollover
③ Rollover
Downlap geometry in D
D
① Rollover
② Rollover
③ Rollover
④ Rollover
Downlap geometry in E
E
① Rollover
② Rollover
③ Rollover
④ Rollover
⑤ Rollover
Downlap geometry in F
F
① Rollover
② Rollover
③ Rollover
④ Rollover
⑤ Rollover
⑥ Rollover
G
IV 1
Fluvial
H
IV 2
Estuarine
IV 1

direction (southwest) are thought to have reduced accommodation towards the northeast, resulting in bypass and erosion (cf. Christie-Blick and Driscoll 1995; Shanley and McCabe 1995). A decrease in the amount of tilting is interpreted to have resulted in deepening and flooding in the incised valley, and in the upward transition from fluvial to estuarine sedimentation. Analogous interpretations regarding sequence-boundary formation and controls on incised-valley fill have been suggested for coarse-grained siliciclastic deposits of the early Tertiary Alpine foreland basin in southeastern France. In that area, incision is thought to be caused by uplift and tilting during growth of underlying basement-cored fault-propagation anticlines (Gupta 1997).

Evidence Against a Change in Siliciclastic Source

A change in siliciclastic source alone cannot account for both a deflection in the rollover position with time (map view) and the observed stratigraphic geometry (cross section). Although a systematic clockwise rotation in point or line sources can create a change in rollover orientation consistent with the observed geometry of the Cozzette Sandstone, it cannot explain tilted geometries observed in cross section. Hence, three-dimensional tectonic tilting is required.

Mechanisms of Tilting

Faulting at depth and shallow compaction provide mechanisms for syndepositional to postdepositional tilting during accumulation of the Cozzette Sandstone. Aside from major Laramide-reactivated Pennsylvanian high-angle blind normal faults, which are interpreted to have led to the development of anticlines in the basin (Johnson 1989; Grout and Verbeek 1992), faulting has not been studied in detail in the interior of the Piceance. Where observed, faults are minor, trending exclusively to the north to north-northwest, and restricted to the basin margins (Johnson 1989). Although accommodation change in the Cozzette cannot be correlated with any particular late Campanian fault or family of faults, brittle deformation at depth is hypothesized to be the primary mechanism of tilting. Salt motion may also have played a role, though preserved evaporites of the Pennsylvanian–Permian Paradox evaporite basin pinch out more than 80 km (50 mi) to the southwest of the study area (Baltz 1957; Baars and Stevenson 1981; Nuccio and Condon 1996; Trudgill 2011).

Differential compaction, which is controlled primarily by lithology and burial depth (Bond and Kominz 1984), would have augmented other mechanisms. The interaction of compaction and tilting in the Cozzette Sandstone is currently being numerically modeled; details of that work will be published elsewhere.

CONCLUSIONS

The late Campanian aged Cozzette Sandstone, southern Piceance basin, eastern Book Cliffs of northwestern Colorado, consists of twelve lithofacies organized into six lithofacies assemblages, deposited in shallow marine, marginal marine, and nonmarine depositional environments. Shallow marine deposits are arranged into six offlapping wave-dominated parasequences, with offlap interpreted to represent bypass. Shallow marine cycles, which are separated by flooding surfaces and grouped into three progradational to aggradational cycles, formed with an average duration of $\sim$ 221 kyr. Shoreface–foreshore–swamp deposits are inferred to have tilted in three dimensions during deposition, producing a marked change in the trend of the clinoform rollover from northeast to east. Overlying fluvial and estuarine deposits are contained either within one composite incised valley fill or within two distinct fills, and are interpreted to be floored by tectonically induced sequence boundaries. Incised-valley-fill deposits trend southwest, are interpreted to reflect tilting in that direction, and accumulated in $\sim$ 1.46 Myr.

Syndepositional and postdepositional tilting in the southern Piceance basin, rather than the interactions between eustasy and regional patterns of flexural subsidence, is interpreted to have controlled accumulation of the Cozzette Sandstone. Subsidence is inferred to have been caused principally by faulting at depth, as well as shallow compaction trends. These new insights concerning the relationship between deposition and deformation cast doubt on conventional sequence stratigraphic interpretation of patterns of sedimentation in terms of the essentially one-dimensional concept of relative sea-level change.

ACKNOWLEDGMENTS

The authors thank the American Association of Petroleum Geologists Grants-in-Aid of Research, Sigma Xi Grants-in-Aid of Research, Columbia's Department of Earth and Environmental Sciences, and the Seismology Geology Tectonophysics Division of Lamont-Doherty Earth Observatory for financial support for field work (Madof). We are especially grateful to the Colorado Oil and Gas Commission (http://dnrwebmapgdev.state.co.us/mg2012app/) for access to public well-log data, to Steven P. Cumella for sharing outcrop photographs, to Mark A. Kirschbaum for advice regarding locations of measured sections, and to William Sanders for lending digital video equipment and coordinating the helicopter survey. We thank Diane L. Kamola, Daniel F. Stockli, and Anthony W. Walton for their input to an earlier version of the interpretation, John J. Kirrane, John R. Schneider, and Mustapha Zater for their assistance in the field, Todd D. Bowers for technical support, and Simon Lang, Morgan D. Sullivan, Ashley D. Harris, and Jacob A. Covault for stimulating and thought-provoking suggestions regarding the manuscript. We would also like to thank reviewers Peter M. Burgess and Andrew D. Miall for their comments and suggestions. Lamont-Doherty Earth Observatory Contribution Number 7872.

REFERENCES

Ainsworth, R.B., and Pattison, S.A.J., 1994, Where have all the lowstands gone? Evidence for attached lowstand systems tracts in the western interior of North America: Geology, v. 22, p. 415–418.

Ambrose, W.A., and Ayers, W.B., Jr., 2007, Geologic controls on transgressive–regressive cycles in the upper Pictured Cliffs Sandstone and coal geometry in the lower Fruitland Formation, northern San Juan basin, New Mexico and Colorado: American Association of Petroleum Geologists, Bulletin, v. 91, p. 1099–1122.

Aschoff, J.L., and Steel, R.J., 2011a, Anatomy and development of a low-accommodation clastic wedge, upper Cretaceous, Cordilleran foreland basin, USA: Sedimentary Geology, v. 236, p. 1–24.

Aschoff, J., and Steel, R., 2011b, Anomalous clastic wedge development during the Sevier–Laramide transition, North American Cordilleran foreland basin, USA: Geological Society of America, Bulletin, v. 123, p. 1822–1835.

Atchley, S.C., Nordt, L.C., and Dworkin, S.I., 2004, Eustatic control on alluvial sequence stratigraphy: a possible example from the Cretaceous–Tertiary transition of the Tornillo basin, Big Bend National Park, West Texas, U.S.A.: Journal of Sedimentary Research, v. 74, p. 391–404.

Baars, D.L., and Stevenson, G.M., 1981, Tectonic evolution of the Paradox Basin, Utah and Colorado, *in* Wiegand, D.L., ed., Geology of the Paradox Basin: Rocky Mountain Association of Geologists, Field Conference, p. 23–31.

Baltz, E.H., 1957, Distribution and thickness of salt in the Paradox Basin of southwestern Colorado and southeaster Utah, a preliminary report: U.S. Geological Survey, Trace Elements Investigations Report, TEM-706, 42 p.

Bera, M.K., Sarkar, A., Chakraborty, P.P., Loyal, R.S., Sanyal, P., 2008, Marine to continental transition in Himalayan foreland: Geological Society of America, Bulletin, v. 120, p. 1214–1232.

Bond, G.C., and Kominz, M.A., 1984, Construction of tectonic subsidence curves for the early Paleozoic miogeocline, southern Canadian Rocky Mountains: implications for subsidence mechanisms, age of breakup, and crustal thinning: Geological Society of America, Bulletin, v. 95, p. 155–173.

Buillit, N., Lallier-Vergès, E., Pradier, B., and Nicolas, G., 2002, Coal petrographic genetic units in deltaic-plain deposits of the Campanian Mesa Verde Group (New Mexico, USA): International Journal of Coal Geology, v. 51, p. 93–110.

Burgess, P.M., Gurnis, M., and Moresi, L., 1997, Formation of sequences in the cratonic interior of North America by interaction between mantle, eustatic, and stratigraphic processes: Geological Society of America, Bulletin, v. 108, p. 1515–1535.

Castle, J.W., 2001, Foreland-basin sequence response to collisional tectonism: Geological Society of America, Bulletin, v. 113, p. 801–812.

Catuneanu, O., Sweet, A.R., and Miall, A.D., 2000, Reciprocal stratigraphy of the Campanian–Paleocene western interior of North America: Sedimentary Geology, v. 134, p. 235–255.

Christie-Blick, N., and Driscoll, N.W., 1995, Sequence stratigraphy: Annual Review of Earth and Planetary Sciences, v. 23, p. 451–478.

Clifton, H.E., Hunter, R.E., and Phillips, R.L., 1971, Depositional structures and processes in the non-barred high energy nearshore: Journal of Sedimentary Petrology, v. 41, p. 651–670.

Collins, B.A., 1976, Coal deposits of the eastern Piceance basin, *in* Murray, D.K., ed., Geology of Rocky Mountain Coal: Colorado Geological Survey, Department of Natural Resources, Symposium Proceedings, p. 29–43.

Cross, T.A., 1986, Tectonic controls of foreland basin subsidence and Laramide style deformation, western United States, *in* Allen P.A., and Homewood, P., eds., Foreland Basins: International Association of Sedimentologists, Special Publication 8, p. 15–40.

Cumella, S.P., and Scheevel, J., 2008, The influence of stratigraphy and rock mechanics on Mesaverde gas distribution, Piceance basin, Colorado, *in* Cumella, S.P., Shanley, K.W., and Camp, W.K., eds., Understanding, Exploring, and Developing Tight-Gas Sands, American Association of Petroleum Geologists, Hedberg Series, no. 3, p. 137–155.

DeCelles, P.G., 2004, Late Jurassic to Eocene evolution of the Cordilleran thrust belt and foreland basin system, western U.S.A.: American Journal of Science, v. 304, p. 105–168.

DeCelles, P.G., and Coogan, J.C., 2006, Regional structure and kinematic history of the Sevier fold-and-thrust belt, central Utah: Geological Society of America, Bulletin, v. 118, p. 841–864.

DeCelles, P.G., Lawton, T.F., and Mitra, G., 1995, Thrust timing, growth of structural culminations, and synorogenic sedimentation in the type Sevier orogenic belt, western United States: Geology, v. 23, p. 699–702.

Dickinson, W.R., and Snyder, W.S., 1978, Plate tectonics of the Laramide orogeny, *in* Matthews, V., ed., Laramide Folding Associated with Block Faulting in the Western United States: Geological Society of America, Memoir 151, p. 355–366.

Dott, R.H., Jr., and Bourgeois, J., 1982, Hummocky stratification: significance of its variable bedding sequences: Geological Society of America, Bulletin, v. 93, p. 663–680.

Edwards, C.M., Hodgson, D.M., Flint, S.S., and Howell, J.A., 2005a, Contrasting styles of shelf sediment transport and deposition in a ramp margin setting related to relative sea-level change and basin floor topography, Turonian (Cretaceous) western interior of central Utah, USA: Sedimentary Geology, v. 179, p. 117–152.

Edwards, C.M., Howell, J.A., and Flint, S.S., 2005b, Depositional and stratigraphic architecture of the Santonian Emory Sandstone of the Mancos Shale: implications for Late Cretaceous evolution of the western interior foreland basin of central Utah, U.S.A.: Journal of Sedimentary Research, v. 75, p. 280–299.

Erdmann, C.E., 1934, The Book Cliffs Coal Field in Garfield and Mesa Counties, Colorado: U.S. Geological Survey, Bulletin 851, 150 p.

Escalona, A., and Mann, P., 2006, Sequence-stratigraphic analysis of Eocene clastic foreland basin deposits in central Lake Maracaibo using high-resolution well correlation and 3-D seismic data: American Association of Petroleum Geologists, Bulletin, v. 90, p. 581–623.

Fisher, D.J., 1936, The Book Cliffs Coal Field in Emery and Grand Counties, Utah: U.S. Geological Survey, Bulletin 852, 104 p.

Fisher, D.L., Erdmann, C.E., and Reeside, J.B., Jr., 1960, Cretaceous and Tertiary Formations of the Book Cliffs, Carbon, Emery, and Grand Counties, Utah, and Garfield and Mesa Counties, Colorado: U.S. Geological Survey, Professional Paper 332, 80 p.

Franczyk, K.J., 1989, Depositional Controls on the Late Campanian Sego Sandstone and Implications for Associated Coal-Forming Environments in the Uinta and Piceance Basins: U.S. Geological Survey, Bulletin 1787-F, 17 p., 2 plates.

Gill, J.R., and Hail, W.J., Jr., 1975, Stratigraphic sections across Upper Cretaceous Mancos Shale–Mesaverde Group boundary, eastern Utah and western Colorado: U.S. Geological Survey, Oil and Gas Investigation Chart, OC-68, 1 sheet.

Gries, R., 1983, Oil and gas prospecting beneath Precambrian of foreland thrust plates in Rocky Mountains: American Association of Petroleum Geologists, Bulletin, v. 67, p. 1–28.

Grout, M.A., and Verbeek, E.R., 1992, Fracture History of the Divide Creek and Wolf Creek Anticlines and its Relation to Laramide Basin-Margin Tectonism, Southern Piceance Basin, Northwestern Colorado: U.S. Geological Survey, Bulletin 1787-Z, 32 p.

Gupta, S., 1997, Tectonic control on paleovalley incision at the distal margin of the early Tertiary Alpine foreland basin, southeastern France: Journal of Sedimentary Research, v. 67, p. 1030–1043.

Hampson, G.J., 2000, Discontinuity surfaces, clinoforms, and facies architecture in a wave-dominated, shoreface–shelf parasequence: Journal of Sedimentary Research, v. 70, p. 325–340.

Hampson, G.J., and Storms, J.E.A., 2003, Geomorphological and sequence stratigraphic variability in wave-dominated, shoreface–shelf parasequences: Sedimentology, v. 50, p. 667–701.

Hampson, G.J., Burgess, P.M., and Howell, J.A., 2001, Shoreface tongue geometry constrains history of relative sea-level fall: examples from Late Cretaceous strata in the Book Cliffs area, Utah: Terra Nova, v. 13, p. 188–196.

Haq, B.U., Hardenbol, J., and Vail, P.R., 1987, Chronology of fluctuating sea levels since the Triassic: Science, v. 235, p. 1156–1167.

Haq, B.U., Hardenbol, J., and Vail, P.R., 1988, Mesozoic and Cenozoic chronostratigraphy and cycles of sea-level change, *in* Wilgus, C.K., Hastings, B.S., Kendall, C.G.St.C., Posamentier, H.W., Ross, C.A., and Van Wagoner, J.C., eds., Sea Level Changes: An Integrated Approach: SEPM, Special Publication 42, p. 71–108.

Helland-Hansen, W., and Martinsen, O., 1996, Shoreline trajectories and sequences: description of variable depositional-dip scenarios: Journal of Sedimentary Research, v. 66, p. 670–688.

Helland-Hansen, W., Steel, R.J., and Sømme, T.O., 2012, Shelf genesis revisited: Journal of Sedimentary Research, v. 82, p. 133–148.

Heller, P.L., Angevine, C.L., and Winslow, N.S., 1988, Two-phase stratigraphic model of foreland-basin sequences: Geology, v. 16, p. 501–504.

Henderson, L.J., Gordon, R.G., and Engebretson, D.C., 1984, Mesozoic aseismic ridges on the Farallon plate and southward migration of shallow subduction during the Laramide orogeny: Tectonics, v. 3, p. 121–132.

Henriksen, S., Helland-Hansen, W., and Bullimore, S., 2011, Relationships between shelf-edge trajectories and sediment dispersal along depositional dip and strike: a different approach to sequence stratigraphy: Basin Research, v. 23, p. 3–21.

Hettinger, R.D., and Kirschbaum, M.A., 2003, Stratigraphy of the Upper Cretaceous Mancos Shale (upper part) and Mesaverde Group in the southern part of the Uinta and Piceance basins, Utah and Colorado: Petroleum Systems and Geologic Assessment of Oil and Gas in the Uinta–Piceance Province, Utah and Colorado, Chapter 12: U.S. Geological Survey, Digital Data Series DDS-69-B, 21 p., 2 plates.

Hood, K.C., and Yurewicz, D.A., 2008, Assessing the Mesaverde basin-centered gas play, Piceance basin, Colorado, *in* Cumella, S.P., Shanley, K.W., and Camp, W.K., eds., Understanding, Exploring, and Developing Tight-Gas Sands: American Association of Petroleum Geologist, Hedberg Series, no. 3, p. 87–104.

Hoy, R.G., and Ridgway, K.D., 2003, Sedimentology and sequence stratigraphy of fan-delta and river-delta deposystems, Pennsylvanian Minturn Formation, Colorado: American Association of Petroleum Geologists, Bulletin, v. 87, p. 1169–1191.

Ito, M., Ishigaki, A., Nishikawa, T., and Saito, T., 2001, Temporal variation in the wavelength of hummocky cross-stratification: implications for storm intensity through the Mesozoic and Cenozoic: Geology, v. 29, p. 87–89.

Johnson, R.C., 1979, Cross section B–B′ of Upper Cretaceous and lower Tertiary rocks, northern Piceance Creek basin, Colorado: U.S. Geological Survey, Miscellaneous Field Studies Map, MF-1129B, 2 plates.

Johnson, R.C., 1986, Structure contour map of the top of the Castlegate sandstone, eastern part of the Uinta basin and the western part of the Piceance Creek basin, Utah and Colorado: U.S. Geological Survey, Miscellaneous Field Studies Map, MF-1826, 2 plates.

Johnson, R.C., 1989, Geologic History and Hydrocarbon Potential of Late Cretaceous Age, Low-Permeability Reservoirs, Piceance Basin, Western Colorado: U.S. Geological Survey, Bulletin 1787–E, 51 p., 2 plates.

Johnson, R.C., 2003, Depositional framework of the Upper Cretaceous Mancos Shale and the lower part of the Upper Cretaceous Mesaverde Group, western Colorado and eastern Utah: Petroleum Systems and Geologic Assessment of Oil and Gas in the Uinta–Piceance Province, Utah and Colorado, Chapter 11: U.S. Geological Survey, Digital Data Series DDS-69-B, 24 p., 1 plate.

Johnson, R.C., Granica, M.P., and Dessenberger, N.D., 1979a, Cross section A–A′ of Upper Cretaceous and lower Tertiary rocks, southern Piceance Creek basin, Colorado: U.S. Geological Survey, Miscellaneous Field Studies Map, MF-1130A, 2 plates.

Johnson, R.C., Granica, M.P., and Dessenberger, N.D., 1979b, Cross section B–B′ of Upper Cretaceous and lower Tertiary rocks, southern Piceance Creek basin, Colorado: U.S. Geological Survey, Miscellaneous Field Studies Map, MF-1130B, 2 plates.

Johnson, R.C., Granica, M.P., and Dessenberger, N.D., 1979c, Cross section C–C′ of Upper Cretaceous and lower Tertiary rocks, southern Piceance Creek basin, Colorado: U.S. Geological Survey, Miscellaneous Field Studies Map, MF-1130C, 2 plates.

Jordan, T.D., 1981, Thrust loads and foreland basin evolution, Cretaceous, Western United States: American Association of Petroleum Geologists, Bulletin, v. 65, 2506–2520.

Kamola, D.L., Madof, A.S., and Zater, M., 2007, Stratal architecture and sequence stratigraphy of the Mount Garfield Formation, Grand Junction area, Colorado: Geological Society of America, Field Trip 424, November 1–3, 31 p., 3 plates.

Kennedy, W.J., Landman, N.H., Cobban, W.A., and Scott, G.R., 2000, Late Campanian (Cretaceous) Heteromorphy Ammonites from the Western Interior of the United States: Bulletin of the American Museum of Natural History, no. 251, 88 p.

Kirschbaum, M.A., and Hettinger, R.D., 2004, Facies analysis and sequence stratigraphic framework of upper Campanian strata (Neslen and Mount Garfield Formations, Bluecastle Tongue of the Castlegate Sandstone, and Mancos Shale), eastern Book Cliffs, Colorado and Utah: U.S. Geological, Survey Digital Data Series DDS-69-G, 40 p., 7 plates.

Lickorish, W.H., and Butler, R.W.H., 1996, Fold amplification and parasequence stacking patterns in syntectonic shoreface carbonates: Geological Society of America, Bulletin, v. 108, p. 966–977.

Liu, S., and Nummendal, D., 2007, Late Cretaceous subsidence in Wyoming: quantifying the dynamic component: Geology, v. 32, p. 397–400.

Madden, D.J., 1989, Stratigraphy, Depositional Environments, and Paleogeography of Coal-Bearing Strata in the Upper Cretaceous Mesaverde Group, Central Grand Hogback, Garfield County, Colorado: U.S. Geological Survey, Professional Paper 1485, 45 p., 2 plates.

Madof, A.S., 2006, Sequence stratigraphic analysis of high frequency sequences: Cozzette Sandstone member, Mount Garfield Formation, Book Cliffs, Colorado [unpublished Master's thesis]: Department of Geology, University of Kansas, Lawrence, Kansas, 137 p., 8 plates.

Martinson, V.S., Heller, P.L., and Frerichs, W.E., 1998, Distinguishing middle Late Cretaceous tectonic events from regional sea-level change using foraminiferal data from the U. S. western interior: Geological Society of America, Bulletin, v. 110, p. 259–268.

Mederos, S., Tikoff, B., and Bankey, V., 2005, Geometry, timing, and continuity of the Rock Springs uplift, Wyoming, and Douglas Creek arch, Colorado: implications for uplift mechanisms in the Rocky Mountain foreland, U.S.A.: Rocky Mountain Geology, v. 40, p. 167–191.

Mellere, D., 1996, Seminoe 3, a tidally influenced lowstand wedge and its relationship with subjacent highstand and overlying transgressive deposits, Haystack Mountains Formation, Cretaceous western interior, Wyoming (USA): Sedimentary Geology, v. 103, p. 249–272.

Mellere, D., and Steel, R., 1995, Variability of lowstand wedges and their distinction form forced-regressive wedges in the Mesaverde Group, southeast Wyoming: Geology, v. 23, p. 803–806.

Miall, A., 2014, The emptiness of the stratigraphic record: a preliminary evaluation of missing time in the Mesaverde Group, Book Cliffs, Utah, U.S.A.: Journal of Sedimentary Research, v. 84, p. 457–469.

Miller, K.G., Sugarman, P.J., Browning, J.V., Kominz, M.A., Olsson, R.K., Feigenson, M.D., and Hernandez, J.C., 2004, upper Cretaceous sequences and sea-level history, New Jersey coastal plain: Geological Society of America, Bulletin, v. 116, p. 368–393.

Miller, K.G., Kominz, M.A., Browning, J.V., Wright, J.D., Mountain, G.S., Katz, M.E., Sugarman, P.J., Cramer, B.S., Christie-Blick, N., and Pekar, S.F., 2005a, The Phanerozoic record of global sea-level change: Science, v. 301, p. 1293–1298.

Miller, K.G., Wright, J.D., and Browning, J.V., 2005b, Visions of ice sheets in a greenhouse world: Marine Geology, v. 217, p. 215–231.

Mitchum, R.M., Jr., Vail, P.R., and Thompson, S., III, 1977, Seismic stratigraphy and global changes of sea level, Part 2: the depositional sequence as a basic unit for stratigraphic analysis, *in* Payton, C.E., ed., Seismic Stratigraphy Applications to Hydrocarbon Exploration: American Association of Petroleum Geologists, Memoir 26, p. 53–62.

Mitchum, R.M., Jr., and Van Wagoner, J.C., 1991, High-frequency sequences and their stacking patterns: sequence-stratigraphic evidence of high-frequency eustatic cycles: Sedimentary Geology, v. 70, p. 131–160.

Nuccio, V.F., and Condon, S.M., 1996, Burial and Thermal History of the Paradox Basin, Utah and Colorado, and Petroleum of the Middle Pennsylvanian Paradox Formation: U.S. Geological Society, Bulletin 2000-O, 41 p.

Ogg, J.G., Agterberg, F.P., and Gradstein, F.M., 2004, The Cretaceous Period, *in* Gradstein, F.M., Ogg, J.G., and Smith, A.G., eds., A Geologic Time Scale 2004: Cambridge, Cambridge University Press, p. 344–383.

Patterson, P.E., Kronmueller, K., and Davies, T.D., 2003, Sequence stratigraphy of the Mesaverde group and Ohio Creek conglomerate, northern Piceance basin, Colorado, *in* Peterson, K.M., Olson, T.M., and Anderson, D.S., eds., Piceance Basin 2003 Guidebook: Rocky Mountain Association of Geologists, p. 115–128.

Pattison, S.A.J., 1995, Sequence stratigraphic significance of sharp-based lowstand shoreface deposits, Kenilworth Member, Book Cliffs, Utah: American Association of Petroleum Geologists, Bulletin, v. 79, p. 444–462.

Pekar, S.F., Christie-Blick, N., Miller, K.G., and Kominz, M.A., 2003, Quantitative constraints on the origin of stratigraphic architecture at passive continental margins: Oligocene sedimentation in New Jersey, U.S.A.: Journal of Sedimentary Research, v. 73, p. 227–245.

Prince, G.D., and Burgess, P.M., 2013, Numerical modeling of falling-stage topset aggradation: implications for distinguishing between forced and unforced regressions in the geological record: Journal of Sedimentary Research, v. 83, p. 767–781.

Posamentier, H.W., and Vail, P.R., 1988, Eustatic controls on clastic deposition II, sequence and systems tract models, *in* Wilgus, C.K., Hastings, B.S., Kendall, C.G.St.C., Posamentier, H.W., Ross, C.A., and Van Wagoner, J.C., eds., Sea Level Changes: an Integrated Approach: SEPM, Special Publication 42, p. 125–154.

Posamentier, H.W., Jervey, M.T., and Vail, P.R., 1988, Eustatic controls on clastic deposition I: conceptual framework, *in* Wilgus, C.K., Hastings, B.S., Kendall, C.G.St.C., Posamentier, H.W., Ross, C.A., and Van Wagoner, J.C., eds., Sea Level Changes: an Integrated Approach: SEPM, Special Publication 42, p. 109–124.

Posamentier, H.W., Allen, G.P., James, D.P., and Tesson, M., 1992, Forced regressions in a sequence stratigraphic framework: concepts, examples, and exploration significance: American Association of Petroleum Geologists, Bulletin, v. 76, p. 1687–1709.

Posamentier, H.W., and Allen, G.P., 1993, Siliciclastic sequence stratigraphic patterns in foreland ramp-type basins: Geology, v. 21, p. 455–458.

Reineck, H.E., and Singh, I.B., 1980, Depositional Sedimentary Environments, with Reference to Terrigenous Clastics: New York, Springer-Verlag, 549 p.

Reinson, G.E., 1984, Barrier-island and associated strand-plain systems, *in* Walker, R.G., ed., Facies Models, Second Edition: Geological Association of Canada, p. 119–140.

Robinson Roberts, L.N., and Kirschbaum, M.A., 1995, Paleogeography of the Late Cretaceous of the Western Interior of Middle North America: Coal Distribution and Sediment Accumulation: U.S. Geological Survey, Professional Paper 1561, 115 p.

Shanley, K.W., and McCabe, P.J., 1995, Sequence stratigraphy of Turonian–Santonian strata, Kaiparowits Plateau, southern Utah, U.S.A.: implications for regional correlation and foreland basin evolution, *in* Van Wagoner, J.C., and Bertram, G.T., eds., Sequence Stratigraphy of Foreland Basin Deposits: Outcrop and Subsurface Examples from the Cretaceous of North America, American Association of Petroleum Geologists, Memoir 64, p. 103–136.

Sixsmith, P.J., Hampson, G.J., Gupta, S., Johnson, H.D., and Fofana, J.F., 2008, Facies architecture of a net transgressive sandstone reservoir analog: the Cretaceous Hosta Tongue, New Mexico: American Association of Petroleum Geologists, Bulletin, v. 92, p. 513–547.

Storms, J.E.A., and Hampson, G.J., 2005, Mechanisms for forming discontinuity surfaces within shoreface–shelf parasequences: sea level, sediment supply, or wave regime?: Journal of Sedimentary Research, v. 75, p. 67–81.

Thomas, R.G., Smith, D.G., Wood, J.M., Visser, J., Calverley-Range, E.A., and Koster, E.H., 1987, Inclined heterolithic stratification: terminology, description, interpretation and significance: Sedimentary Geology, v. 53, p. 123–179.

Trudgill, B.D., 2011, Evolution of salt structures in the northern Paradox Basin: controls on evaporite deposition, salt wall growth and supra-salt stratigraphic architecture: Basin Research, v. 23, p. 208–238.

Vail, P.R., 1987, Seismic stratigraphy interpretation using sequence stratigraphy, part 1: seismic stratigraphy interpretation procedure, *in* Bally, A.W., ed., Atlas of Seismic Stratigraphy: American Association of Petroleum Geologists, Studies in Geology 27, v. 1, p. 1–10.

Vail, P.R., Mitchum, R.M., Jr., and Thompson, S., III, 1977, Seismic stratigraphy and global changes of sea level, part 4: global cycles of relative changes of sea level, *in* Payton, C.W., ed., Seismic Stratigraphy: Applications to Hydrocarbon Exploration: American Association of Petroleum Geologists, Memoir 26, p. 83–97.

Vakarelov, B.K., and Bhattacharya, J.P., 2009, Local tectonic control on parasequence architecture: Second Frontier Sandstone, Powder River basin, Wyoming: American Association of Petroleum Geologists, Bulletin, v. 93, p. 295–327.

Van Wagoner, J.C., 1985, Reservoir facies distribution as controlled by sea-level change [Abstract]: SEPM, Mid-Year Meeting, Golden, Colorado, August 11–14, p. 91–92.

Van Wagoner, J.C., 1991a, American Association of Petroleum Geologists, field conference: sequence-stratigraphy applications to shelf-sandstone reservoirs: outcrop to subsurface examples, *in* Van Wagoner, J.C., Jones, C.R., Taylor, D.R., Nummedal, D., Jennette, D.C., and Riley, G.W., eds., Sequence Stratigraphy Applications to Shelf Sandstone Reservoirs: Outcrop to Subsurface Examples: American Association of Petroleum Geologists, Field Conference, September 21–28, p. 1–6.

Van Wagoner, J.C., 1991b, High-frequency sequence stratigraphy and facies architecture of the Sego sandstone in the Book Cliffs of western Colorado and eastern Utah, *in* Van Wagoner, J.C., Jones, C.R., Taylor, D.R., Nummedal, D., Jennette, D.C., and Riley, G.W., eds., Sequence Stratigraphy Applications to Shelf Sandstone Reservoirs: Outcrop to Subsurface Examples: American Association of Petroleum Geologists, Field Conference, September 21–28, p. 1–10.

Van Wagoner, J.C., 1995, Sequence stratigraphy and marine to nonmarine facies architecture of foreland basin strata, Book Cliffs, Utah, U.S.A., *in* Van Wagoner, J.C., and Bertram, G.T., eds., Sequence Stratigraphy of Foreland Basin Deposits: Outcrop and Subsurface Examples from the Cretaceous of North America: American Association of Petroleum Geologists, Memoir 64, p. 137–223.

Van Wagoner, J.C., Posamentier, H.W., Mitchum, R.M., Vail, P.R., Sarg, J.F., Loutit, T.S., and Hardenbol, J., 1988, An overview of sequence stratigraphy and key definitions, *in* Wilgus, C.K., Hastings, B.S., Kendall, C.G.St.C., Posamentier, H.W., Ross, C.A., and Van Wagoner, J.C., eds., Sea Level Changes: an Integrated Approach: SEPM, Special Publication 42, p. 39–45.

Van Wagoner, J.C., Mitchum, R.M., Jr., Campion, K.M., and Rahmanian, V.D., 1990, Siliciclastic Sequence Stratigraphy in Well Logs, Cores, and Outcrops: Association of Petroleum Geologists, Methods in Exploration 7, 55 p.

Varban, B.L., and Plint, A.G., 2008, Sequence stacking patterns in the western Canada foredeep: influence of tectonics, sediment loading and eustasy on deposition of the upper Cretaceous Kaskapau and Cardium formation: Sedimentology, v. 55, p. 395–421.

Walker, R.G., and Plint, A.G., 1992, Wave- and storm-dominated shallow marine systems, *in* Walker, R.G., and James, N.P., eds., Facies Models: Response to Sea Level Change, p. 219–238.

Warner, D.L., 1964, Mancos–Mesaverde (upper Cretaceous) intertonguing relations southeast Piceance basin, Colorado: American Association of Petroleum Geologists, Bulletin, v. 48, p. 1091–1107.

Willis, A., 2000, Tectonic control of nested sequence architecture in the Sego sandstone, Neslen Formation and upper Castlegate sandstone (Upper Cretaceous), Sevier foreland basin, Utah, USA: Sedimentary Geology, v. 136, p. 277–317.

Young, R.G., 1955, Sedimentary facies and intertonguing in the upper Cretaceous of the Book Cliffs, Utah–Colorado: Geological Society of America, Bulletin, v. 66, p. 177–202.

Young, R.G., 1966, Stratigraphy of coal-bearing rocks of Book Cliffs, Utah–Colorado, *in* Hamblin, W.K., and Rigby, J.K., eds., Central Utah Coals: Utah Geological and Mineralogical Survey, Bulletin 80, p. 7–21.

Yurewicz, D.A., Bohacs, K.M., Kendall, J., Klimentidis, R.E., Kronmueller, K., Meurer, M.E., Ryan, T.C., and Yeakel, J.D., 2008, Controls on gas and water distribution, Mesaverde basin-centered gas play, Piceance basin, Colorado, *in* Cumella, S.P., Shanley, K.W., and Camp, W.K., eds., Understanding, Exploring, and Developing Tight-Gas Sands: American Association of Petroleum Geologist, Hedberg Series, no. 3, p. 105–136.

Zapp, A.D., and Cobban, W.A., 1960, Some Late Cretaceous Strand Lines in Northwestern Colorado and Northeastern Utah: U.S. Geological Survey Professional Paper 400-B, p. 246–249.

Received 18 March 2014; accepted 2 January 2015.